

# Modeling seismic response of a full-scale cold-formed steel-framed building



Jiazen Leng <sup>a,\*</sup>, Kara D. Peterman <sup>a,1</sup>, Guanbo Bian <sup>a</sup>, Stephen G. Buonopane <sup>b</sup>, Benjamin W. Schafer <sup>a</sup>

<sup>a</sup> Department of Civil Engineering, Johns Hopkins University, Baltimore, MD, USA

<sup>b</sup> Department of Civil and Environmental Engineering, Bucknell University, Lewisburg, PA, USA

## ARTICLE INFO

### Article history:

Received 1 December 2016

Revised 9 August 2017

Accepted 4 October 2017

Available online 20 October 2017

## ABSTRACT

The objective of this paper is to present finite element modeling protocols and validation studies for the seismic response of a two-story cold-formed steel-framed building with oriented strand board sheathed shear walls. Recently, shake table testing of this building was completed by the authors. The building provides an archetype for modern details of cold-formed steel construction, and provides benchmarks for the seismic response of the building system, subsystem, and components. The seismic response of buildings framed from cold-formed steel has seen little study in comparison with efforts on isolated members and shear walls. Validated building-scale models are needed to expand our understanding of the seismic response of these systems. Finite element models corresponding to the archetype building during its various test phases are developed in OpenSees and detailed herein. For cold-formed steel framed buildings accurate seismic models require consideration of components beyond the isolated shear walls, e.g. the stiffness and capacity of the gravity framing is included in the model. Such decisions require model refinement beyond what is typically performed and details for completing this effort accurately and efficiently are described herein. In addition, nonstructural components, including exterior sheathing of the gravity framing, interior gypsum sheathing for the shear walls and gravity framing, and interior partition walls, are included in the building model based on nonlinear surrogate models that utilize experimental characterization of member-fastener-sheathing response. Comparisons between the developed models and testing for natural period, story drift, accelerations, and foundation hold-down forces validate the model. Performance of the tested archetype building is better than predicted by design or typical engineering assumptions. The model developed herein provides insights into how the building achieves its beneficial performance and will be used to further quantify the lateral resistance of each subsystem and the extent of their coupling. In addition, the protocols used to develop the model herein provide a first examination of the necessary modeling characteristics for wider archetype studies of cold-formed steel-framed buildings and the development and substantiation of seismic response modification coefficients.

© 2017 Elsevier Ltd. All rights reserved.

## 1. Introduction

Buildings framed from cold-formed steel (CFS) are increasingly being specified due to their low cost, high material efficiency, short cycle times in manufacturing and construction, non-combustibility, and other factors. CFS-framed buildings typically

consist of repetitive series of closely-spaced lipped channel CFS members: studs for walls, joists for floors; fastened together by screws and/or welds, and further stiffened with strap, sheet, or sheathing panels to resist applied loads. CFS framing is also used extensively in non-structural applications such as interior partition walls and exterior curtain walls, but this application is not the focus of the work herein. Research and design experience has grown for the use of CFS as the load-bearing system for gravity and lateral loads in buildings [1]. Modeling the seismic response of CFS-framed buildings is the subject of this paper.

The work presented herein is part of a multi-year research project to advance understanding of CFS-framed buildings in seismic events under the title: Enabling Performance-Based Seismic Design of Multi-Story Cold-Formed Steel Structures, funded by the U.S.

\* Corresponding author at: Department of Mechanical Engineering, McGill University, 817 Sherbrooke Street West, Montreal, QC H3A 0C3, Canada.

E-mail addresses: [jiazen.leng@mcgill.ca](mailto:jiazen.leng@mcgill.ca) (J. Leng), [kdpeterman@umass.edu](mailto:kdpeterman@umass.edu) (K.D. Peterman), [bian@jhu.edu](mailto:bian@jhu.edu) (G. Bian), [sbuonopane@bucknell.edu](mailto:sbuonopane@bucknell.edu) (S.G. Buonopane), [schafer@jhu.edu](mailto:schafer@jhu.edu) (B.W. Schafer).

<sup>1</sup> Department of Civil and Environmental Engineering, University of Massachusetts Amherst, Amherst, MA, USA.

National Science Foundation (NSF) and the American Iron and Steel Institute (AISI) and was formally a part of the NSF Network for Earthquake Engineering Simulation (NEES) research program, or in short CFS-NEES [2]. The central focus of the project was full-scale shake table testing and related modeling of a cold-formed steel ledger-framed building with wood structural panel shear walls and floors, known as the CFS-NEES building. Shake table testing of the CFS-NEES building was conducted in the laboratory of the University at Buffalo in the summer of 2013.

Design codes and standards for CFS-framed structures largely focus on component level design [3,4]. However, repetitively framed CFS buildings are recognized in seismic design [5] and supported with provisions for determining the capacity of the assumed lateral force resisting system (LFRS), e.g. shear wall, strap-braced wall, etc. [6,7]. The CFS-NEES testing provided the first experiments on the full-scale seismic system response for these structures. The CFS-NEES building exhibited stiffness and capacity far beyond that of the assumed LFRS, and suffered no permanent drift and only non-structural damage in testing up to maximum considered earthquake levels [8–10]. The testing demonstrated excellent performance, but also highlighted a significant knowledge gap between system performance and current understanding, which is predominately at the component level.

Compared with experimental efforts, modeling the dynamic seismic response of CFS-framed building systems is less explored. Previous research has focused almost exclusively on modeling the assumed LFRS in isolation. For example, the authors modeled the oriented strand board (OSB) sheathed shear walls of the CFS-NEES building with elastic frame finite elements for the shear wall perimeter and nonlinear diagonal braces for the interior, calibrated to match cyclic shear wall tests [11,12] in OpenSees [13]. This phenomenological approach, where isolated shear walls are modeled such that they fit cyclic test data is the most common approach. Similar models have been adopted for CFS-framed steel sheet shear walls [14], corrugated steel sheet shear walls [15], wood sheathed shear walls [16] and walls sheathed with combinations of sheathing including plaster [17,18]. To estimate building seismic response these phenomenological shear wall models are then typically employed in 2D or 3D building models as the only component of the model available for resisting lateral load [11,12,14–18]. A recent notable exception is the model of a small prototype CFS building, completed in SAP 2000 that includes details beyond the isolated shear walls [19].

A higher resolution model, still implemented in OpenSees, for CFS-framed walls with sheathing has also been developed within the CFS-NEES effort [20]. This model employs cyclic data on the local stud-fastener-sheathing response and implements that data as nonlinear springs in a wall model where the members and sheathing are discretely modeled to predict the lateral wall response [21–23]. This method provides a means to predict the lateral cyclic wall response using only local cyclic fastener data, and is flexible enough to allow for different framing details, fastener patterns and spacing, etc. and is adopted herein as a surrogate model for predicting the cyclic performance of walls and floors that have not been explicitly tested as sub-assemblages, as detailed in Section 3.4.

System-level or full building models of the seismic response of CFS-framed buildings are rare, but comparable work in repetitively framed wood construction does exist. Wood-framed structures, which also feature lightweight designs and share common terminology, provide a useful prototype for needed seismic research in CFS-framing [10]. For example, van de Lindt et al. [24,25] modeled an archetype wood building using SAPWood and compared their numerical predictions with test results. Their nonlinear model condensed the response of floors into global translational and rotational degrees of freedom (DOF) smearing all details of the LFRS,

but overall providing reasonable predictions. Advances have continued, including modeling a five-story residential light-frame wood building with discrete nonlinear phenomenological models for each shear wall and performing incremental dynamic analysis (IDA) to assess seismic response modification coefficient for use in design [26].

This paper presents the authors' efforts on high fidelity modeling and seismic analysis of the two-story CFS-NEES archetype building as detailed in the first author's dissertation [27]. Section 2 of this paper briefly overviews the design and construction of the CFS-NEES building. The assumptions, options, and details of the model development for each structural and nonstructural component of the building are addressed in Section 3. Section 4 provides validation of the models and comparison of time history analysis results with full-scale shake table tests. First natural period, story drift, acceleration, and axial force in shear wall hold-downs are selected as the metrics. The performance of the model is discussed, particularly from the perspective of its application in performance-based design evaluations and its use for IDA and the evaluation of seismic response modification coefficients.

## 2. CFS-NEES building design and construction

### 2.1. CFS-NEES building design

The CFS-NEES building was designed as a CFS-framed two-story office building for a high seismic zone in Orange County, California. The building was designed in accordance with the International Building Code (IBC) [28] and thus by reference the load standard ASCE 7 [5], the member standard AISI-S100 [3], and the lateral design standard AISI-S213 [6]. The building was professionally designed with input from an Industrial Advisory Board and the project team.

The design of the CFS-NEES building reflects current state-of-the-practice in CFS-framed construction. The CFS-framed gravity walls relied on an all-steel design philosophy, i.e. bridging is included between studs and sheathing is not considered as bracing. The CFS-framed floors used OSB sheathing and strap for bracing and were hung from the walls using ledger track. The assumed LFRS employs OSB-sheathed shear walls as well as the OSB-sheathed floor and roof. The resulting structural system is depicted in Fig. 1(a). Building dimensions were 15.2 m × 7 m × 5.8 m (49 ft – 9 in. × 23 ft × 19 ft – 3 in.). Additional non-structural features for the perimeter walls included exterior sheathing, exterior insulation finishing system, and interior gypsum. Architectural features also included interior partition walls and two staircases between the first and the second stories (resulting in two cutouts in the floor diaphragm), windows, and doorways as illustrated in Fig. 1(b). A detailed design narrative with complete calculations and drawings is available [29], and construction details of the specimen are also provided in [8].

A key feature of the building was the selection and use of ledger framing for the floor and roof system as advocated by the Industrial Advisory Board based on current practice. In ledger framing, the joists are hung from the top of the studs of the exterior walls via a ledger track and a clip angle, so the joists need not be aligned with the wall studs (see Fig. 2(a)). This framing type also provides a direct load path from the diaphragm to the top track of the walls, but the sheathing of the diaphragm has to be penetrated to allow the passing of a steel strap that connects shear wall chord studs across the floor, as shown in Fig. 2(a).

The selected seismic LFRS for the building was OSB sheathed shear walls. Per ASCE 7-05 [5] this resulted in a seismic response modification coefficient of  $R = 6.5$ , overstrength factor of  $\Omega_o = 3.0$ , and deflection amplification factor of  $C_d = 4.0$ . The seismic design

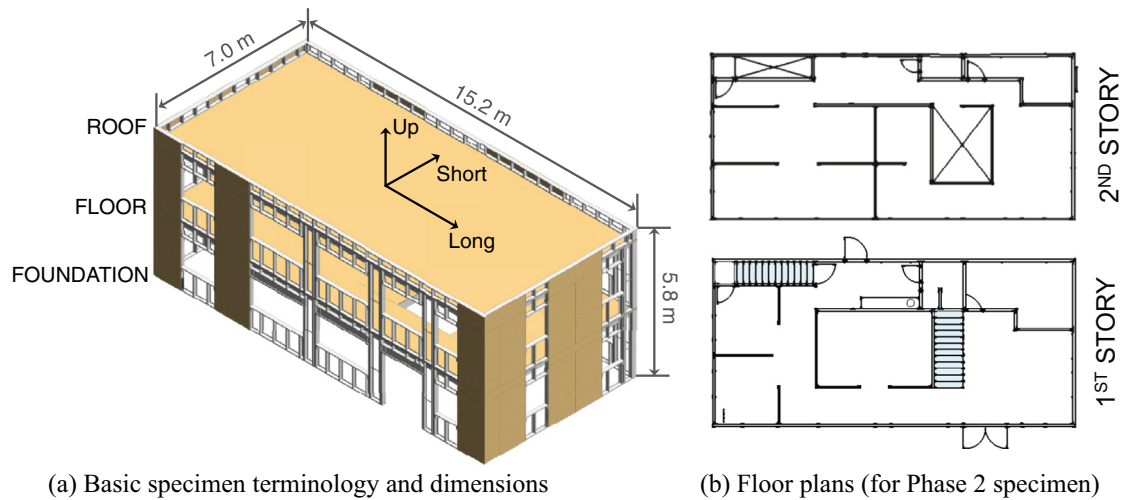


**Fig. 1.** Structural system and architectural plans for the CFS-NEES building.

mass of the building was estimated to be 35100 kg (77500 lbs), resulting in a fundamental period estimate of 0.175 s, and when adjusted by  $R$ , a demand base shear of 49 kN (11 kips). Type I shear walls (as defined in AISI S213 [6]) were adopted in the design and required to meet strength and drift criteria. Typical shear wall design is shown in Fig. 2(b). The CFS steel framing is formed by fastening back-to-back lipped channel chord studs at two ends, single lipped channel field studs and top and bottom tracks together. Simpson S/HDU6 hold-downs were selected for the shear wall chord stud to foundation connection as shown in Fig. 2(c). The back-to-back shear wall chord studs were designed based on ASCE 7 load combinations, including gravity loads and for seismic load the minimum of the amplified (by  $\Omega_o$ ) seismic load, or the maximum load the shear wall can deliver (per AISI S213 [6]) resulting in 600S200-54 studs on the first story and 600S200-43 studs on the second story. The chord studs of the shear walls on the floor level and the roof level are connected via a cold-formed strap directly through the floor and track, fastened to the webs of the shear wall chord studs as shown in Fig. 2(d). The strap tie was sized in accordance with the requirements of AISI S213 [6]. Its installation requires holes to be cut in the sheathing after the floor system is installed. Member sizing details and complete drawings are available in [29].

The floor and roof diaphragms employed CFS joists and OSB sheathing and were initially idealized as flexible according to ASCE 7-05, Section 12.3.1.1 [5]. The diaphragms were also checked as rigid and the envelope of the predicted forces delivered to the shear walls considered in design. Diaphragm perimeter members were sized for the maximum value of the drag force supplied to the shear walls and diaphragm chord forces based on a beam analogy with the chords acting as the tension and compression elements similar to beam flanges. Blocking and strapping in large segments and reinforcing details of staircase openings on the floor diaphragm can be found in the design narrative [29]. An exploded isometric view of the Phase 1 building specimen (only shear wall sheathing is shown) in Fig. 3 illustrates the steel framing of wall lines and diaphragms. Shear wall segments are identified by the story number and their locations on the elevation and are used in later validation. The naming conventions employed here are consistent with the tested specimens.

## 2.2. CFS-NEES building construction phases

The construction and testing of CFS-NEES building was divided into two project phases. The first, Phase 1, examined the

performance of the structural system only, and as such the building specimen was constructed with only structural components: OSB-sheathed CFS-framed shear walls, unsheathed CFS-framed gravity walls, and OSB-sheathed CFS-framed floor and roof diaphragms. After destructive testing the Phase 1 building was demolished and a second nominally identical building, Phase 2, was constructed. The Phase 2 building was non-destructively tested during all construction phases including (a) structural system only, (b) addition of exterior sheathing on gravity walls, (c) addition of gypsum sheathing on interior face of all perimeter walls, (d) addition of interior partition walls, ceilings, and stairs, and (e) addition of exterior insulation finishing system as illustrated in Fig. 4. Destructive testing was completed on Phase 2e, the complete building.

The seismic mass (weight) of the building 35,100 kg (77,500 lbf) was held constant through all phases of testing. The Phase 1/2a (structural-only) building self weight was only 8600 kg (19,000 lbs), and 26,490 kg (58,400 lbs) supplemental seismic mass had to be added in Phase 1/2a [10,29]. Supplemental mass consisted of distributed concrete blocks on the floor and steel plates on the roof. In Phases 2b-2e supplemental mass was removed in equal amounts to the additional self-weight added in the phases such that total seismic mass remained constant. High-fidelity finite element models developed for each phase, as described in the following sections, aim to capture the exact mass, the real geometry and material of the members and subsystems, and to the best accuracy possible depict the nonlinear behavior of the system under ground motion excitations for each phase.

## 3. Development of high-fidelity models for a CFS-framed building

Past efforts in modeling the seismic response of CFS-framed buildings typically rely on simplifications to save computational cost: most commonly the shear wall is idealized as a nonlinear spring or a pair of nonlinear braces [14]; the gravity system is ignored (except as a leaning P – Δ column); and the diaphragms are assumed to be rigid (as a single element in OpenSees [13]). The authors' previous work [11,12] initiated on a similar path, but the predicted results deviated significantly from tested response. For example, predicted first mode period was 100% larger than the measured building natural period even in the Phase 1 (structural only) building with a model using these protocols [2,27]. This realization led to the development of higher fidelity models that reject common modeling simplifications to provide reliable prediction of CFS-framed building system response under

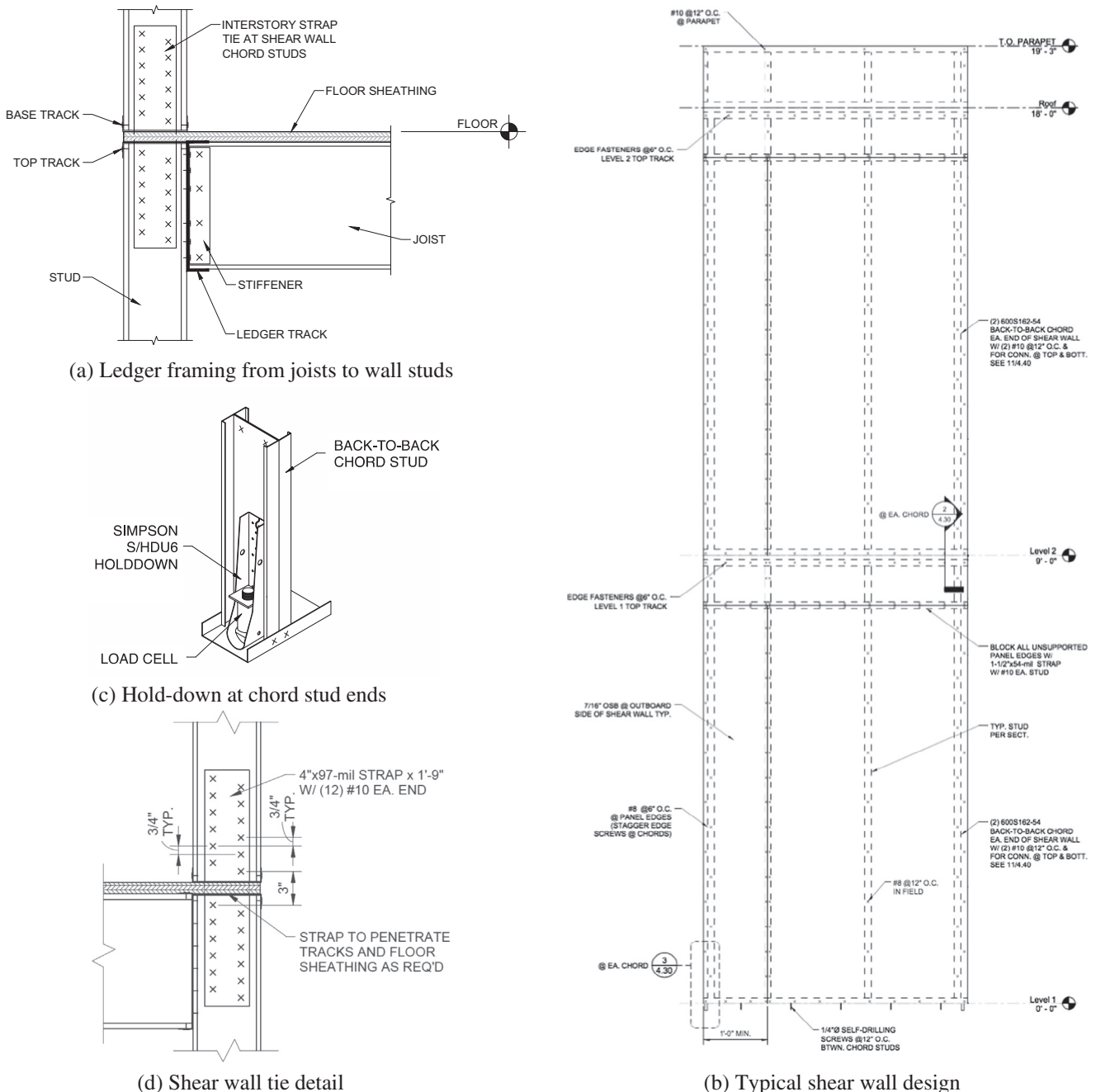


Fig. 2. Selected design details for CFS-NEES building [29].

seismic excitations. These higher fidelity models are the primary focus of the work presented here and detailed in the following sections.

### 3.1. Scope of high-fidelity modeling of CFS-framed building

In the first author's dissertation [27] a large scope of building modeling options was considered, a subset of which are examined in this paper and summarized in Table 1. Two classes of models were developed: state-of-the-practice (P), and state-of-the-art (A). P-models use modeling assumptions consistent with engineering design, strength and stiffness derived from codes and standards, and ignore significant portions of the building. A-models use experimental information developed specifically in the CFS-NEES project, adopt surrogate models to provide predicted

response for non-structural components, and aim to include contributions that reflect all phases (2a-2e) of construction. Two-dimensional (2D) and three-dimensional (3D) models as well as semi-rigid (SD) and rigid diaphragm (RD) models were developed. Comparison of 2D and 3D models and SD and RD models, as well as all other model options, are detailed in [27].

The focus of this work is comparison of the best (highest fidelity) 3D state-of-the-practice (P) and state-of-the-art (A) models. The developed OpenSees models for these cases are depicted in Fig. 5. Careful comparison of the elements in Fig. 5 indicates the major features of the model: (a) considers only the shear walls and mass concentrated in the corners and represents the P-model for all phases, (b) and (e) considers the shear walls and all gravity framing appropriate for Phase 1/2a with the A-model, (c) and (f) introduces panel stiffness into the gravity walls (note

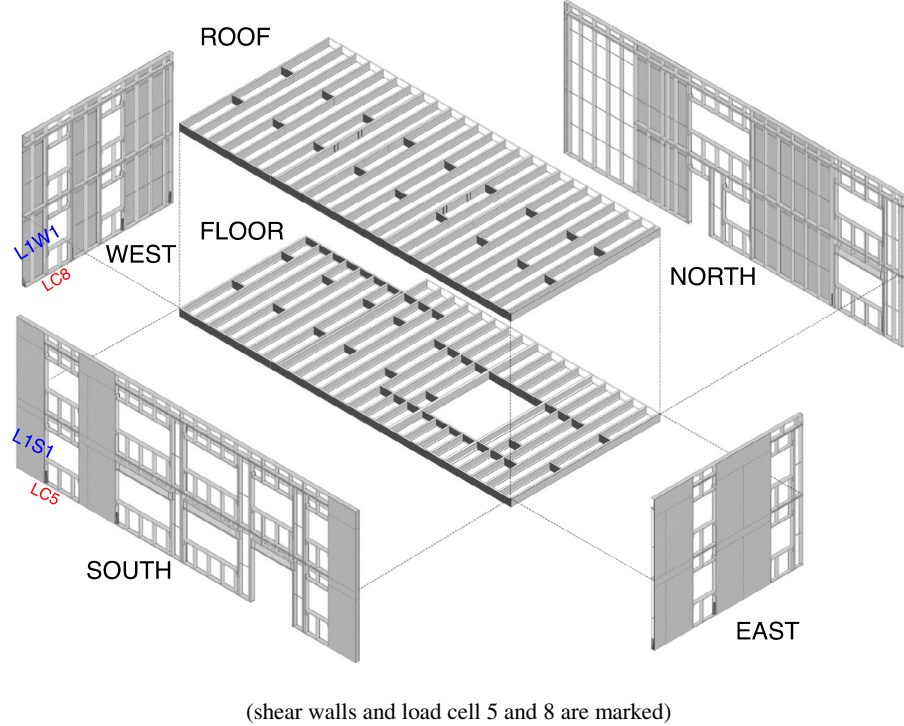


**Fig. 3.** Exploded view of the Phase 1/2a building specimen, framed only with structural components (shear walls and load cell 5 and 8 are marked).

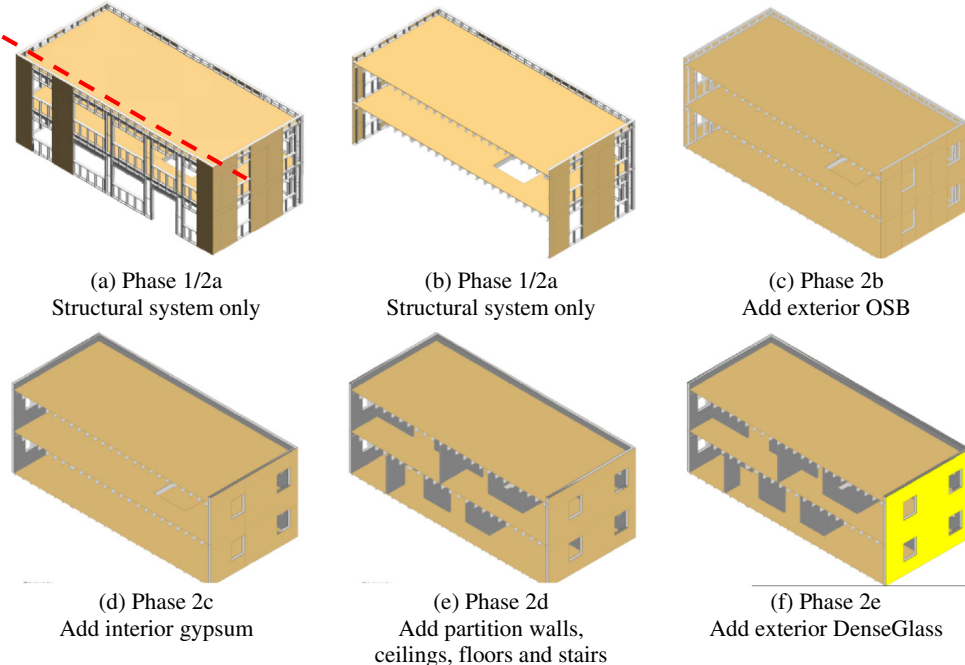


**Fig. 4.** Illustration of construction phases of Phase 2 specimen, shown via cross section views of building specimens (dashed line indicates location of cross section).

the small X members in every opening), appropriate for Phase 2b and 2c A-models, and (d) introduces all the interior framing as needed for Phase 2d. Note, the modeling effort terminated at Phase 2d and the staircases were ignored; however the Phase 2d A-model (A2d-3D-RD-a) was also compared with the complete (Phase 2e) building since tests showed the building's response changed minimally after installing the exterior DensGlass [8]. Details regarding the modeling of each major building component follow.

### 3.2. Modeling of shear walls

The state-of-the-practice (P-) and state-of-the-art (A-) models for the CFS-framed OSB-sheathed shear walls are summarized in this section. The P-model of the shear wall, as depicted in Fig. 5(a) and detailed in Fig. 6(a), uses a pair of diagonal trusses with nonlinear uniaxial material. Conversion of the nonlinear wall force-deformation ( $V - \delta$ ) response into the nonlinear material

**Table 1**

Modeling options for CFS-NEES archetype building.

Component	Property	Option <sup>a</sup>	P-3D-RD-b	State-of-the-Practice		State-of-the-Art		
				Phase 1/2a A1-3D-SD-a	Phase 2b A2b-3D-SD-a	Phase 2c A2c-3D-SD-a	Phase 2d/2e A2d-3D-RD-a	
Shear wall	(Initial) Stiffness	$K(0.4V_{np})$	✓					
		$K(V_{np})$		✓	✓	✓	✓	
		$K(0.2V_{nA})$						
		$K(0.4V_{nA})$						
	Capacity	$V_{nP}$	✓					
		$V_{nA}$		✓	✓	✓	✓	
Hold-down	Hysteresis	EPP						
		Pinching4	✓	✓	✓	✓	✓	
		Whole	✓					
	Panel model	Subpanels		✓	✓	✓	✓	
		Smeared	✓					
		Discrete		✓	✓	✓	✓	
Shear anchors	General	Ignored	✓					
		Included		✓	✓	✓	✓	
Diaphragm	Stiffness	Flexible						
		Rigid	✓					
	Hysteresis	Semi-rigid			✓	✓	✓	
		None	✓		✓	✓	✓	
Gravity exterior walls	General	Pinching4		✓	✓	✓	✓	
	General	None	✓					
		Frame		✓				
Gypsum sheathing	General	Full			✓	✓	✓	
		Ignored	✓		N/A <sup>b</sup>	N/A <sup>b</sup>		
		Included					✓	
Interior walls	General	Ignored	✓		N/A <sup>b</sup>	N/A <sup>b</sup>	N/A <sup>b</sup>	
		Included						✓
Mass distribution	General	Corner	✓					
		Stud ends		✓	✓	✓	✓	

<sup>a</sup> Modeling options considered, see [27] for models and options not summarized here.<sup>b</sup> Not applicable, this element of the building not included in this Phase of construction.

model for the diagonal struts is completed as follows. First, we capture the known  $V - \delta$  response:

$$V = k_t \delta \quad (1)$$

where  $k_t$  is the known tangent stiffness (e.g. from AISI S213 [6] in the P-model). Then we recognize that the lateral stiffness of the pin-connected panel (Fig. 6(a)) of width  $b_o$  and height  $h_o$ , with 2 diagonal struts of area  $A_o$ , may be determined from:

$$V = \left[ 2 \frac{E_{ot} A_o}{L_o} \cos^2 \theta_o \right] \delta \quad (2)$$

where  $L_o = \sqrt{b_o^2 + h_o^2}$ , and  $\cos \theta_o = b_o/L_o$ , and  $E_{ot}$  is the tangent modulus of the uniaxial material in the struts that we seek. Substituting Eq. (1) into Eq. (2) and solving for  $E_{ot}$ :

$$E_{ot} = k_t \frac{L_o^3}{2A_o b_o^2} \quad (3)$$

Thus, the wall tangent stiffness ( $k_t$ ) can readily be converted into a material tangent modulus ( $E_{ot}$ ). In the P-models the capacity and initial stiffness are determined from AISI-S213 [6] which provides the wall strength for these OSB sheathed shear walls, each of length  $b_o$ , as  $V_{nP} = 12.04 \text{ kN/m}$  (825 plf) and noting  $V_{nP} = v_{nP} b_o$ . Stiffness ( $k_t$ ) is determined from the nonlinear deflection expression in AISI S213. To provide an initial linear stiffness for building period prediction etc., the deflection  $\delta$  at  $0.4V_{nP}$  is employed. Two material models are considered for the diagonal trusses, elastic-perfectly-plastic (EPP), as is commonly available in modeling software for engineers, and Pinching4 [30] a unique hysteretic material model

in OpenSees that provides a multi-linear backbone as well as the ability to pinch and degrade the cyclic response. Comparison with isolated shear wall testing indicates the problem of using EPP for CFS-framed OSB sheathed shear walls, specifically due to its lack of consideration for pinching in the unloading/reloading response [31]. As a result, only the Pinching4-based P-model is detailed further here, see [27] for EPP results.

Also for the P-models of the shear walls the boundary steel framing, i.e. studs and track, are modeled with elastic beam-column elements. The connection to the foundation at the hold-down locations is modeled with a pin. Note, the flexibility of the hold-downs is included (in  $k_t$ ) when determining the stiffness in AISI S213; therefore, hold-down stiffness is not explicitly treated and is instead smeared into the shear wall stiffness. Complete details and summary of predicted response for the shear wall P-models are available [11,27] and the most sophisticated of the P-models: P-3D-RD-b is utilized for further comparison herein.

The state-of-the-art “A”-models of the shear wall are depicted in Fig. 6(b). A notable feature of the A-model shear walls is the subdivision of the sheathing board into subpanels. In the P-model all of the shear must be carried to the top or bottom track, while in an actual wall closely spaced fasteners around the perimeter and in the field create shear transfer along the length of the stud and track. In actual framing (see Fig. 3) a number of intermediate members are connected to the shear wall framing, including the ledger as well as window and door headers. By subdividing the shear wall these secondary load paths are allowed in the model and the interaction between the shear walls and the rest of the framing can be considered. For the A-models, the use of subpanels in the shear wall requires an extension to Eq.'s (1)–(3). It is assumed that an

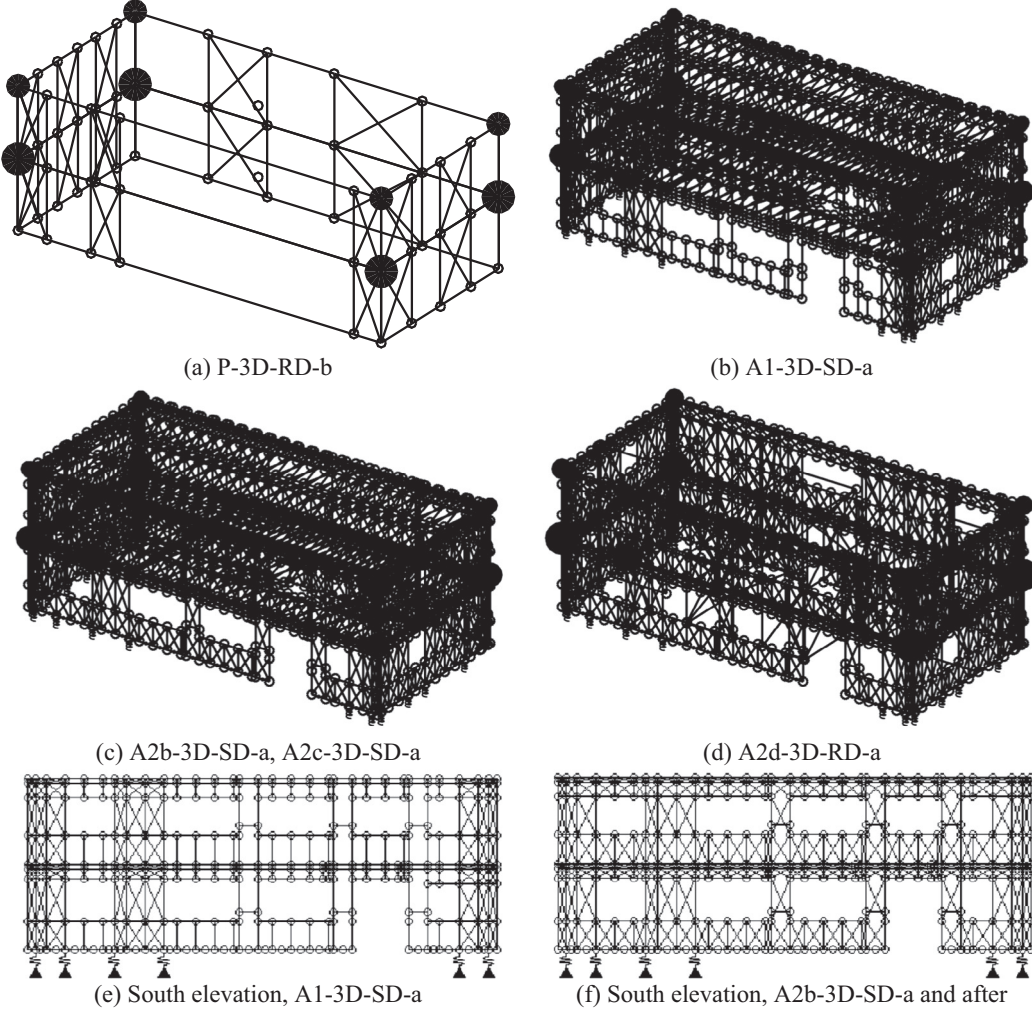


**Fig. 5.** Example 3D OpenSees Models for Building Analysis.

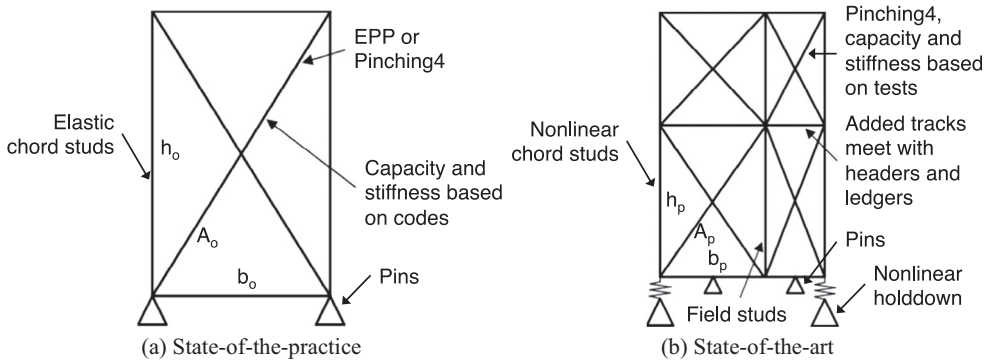


**Fig. 6.** Comparison of modeling strategies: state-of-the-practice vs. state-of-the-art shear wall models.

equivalent shear stress,  $\tau$ , and shear strain,  $\gamma$ , are constant in the shear wall. For any subpanel of dimensions  $b_p \times h_p$  within the shear wall, assuming a state of constant equivalent shear stress implies:

$$\tau = V/(b_o t) \text{ and } \tau_p = \tau \therefore V_p/(b_p t) = V/(b_o t) \quad (4)$$

where  $V_p$  is the lateral force in the subpanel. Assuming constant equivalent shear strain:

$$\gamma = \delta/h_o \text{ and } \gamma_p = \gamma \therefore \delta_p/h_p = \delta/h_o \quad (5)$$

where  $\delta_p$  is the lateral displacement of the subpanel. The lateral stiffness of the subpanel is known, and is similar to Eq. (2):

$$V_p = \left[ 2 \frac{E_{pt} A_p}{L_p} \cos^2 \theta_p \right] \delta_p \quad (6)$$

where  $L_p = \sqrt{b_p^2 + h_p^2}$ , and  $\cos \theta_p = b_p/L_p$ , and  $E_{pt}$  is the tangent modulus of the uniaxial material in the subpanel diagonal struts that we employ in the model. Substituting Eq. (1), (4), and (5) into Eq. (6) and solving for  $E_{pt}$ :

$$E_{pt} = k_t \frac{L_p^3}{2A_p b_p^2} \frac{b_p}{b_o} \frac{h_o}{h_p} \quad (7)$$

With this expression the tangent modulus for any strut can be determined from the overall wall response. Further, Eq. (7) reduces to Eq. (3) when  $b_p = b_o$  and  $h_p = h_o$ .

In the A-models the  $V-\delta$  response is based on shear wall tests [31], e.g. see Fig. 7. The capacity of each shear wall ( $V_{nA}$ ) is based on the average tested value ( $v_{nA} = 14.78 \text{ kN/m}$  (1013 plf) from [31]). The initial stiffness is calculated from the  $\delta$  at  $0.2V_{nA}$  to provide a more accurate approximation when comparing to the white noise excitation at  $0.1 \text{ g}$  used in the experiments. The nonlinear hysteretic shear wall response, as idealized using the Pinching4 model for the entire shear wall, is compared with a typical test in Fig. 7(b), see [27,31] for further comparison. Note, deflections from the hold-downs are isolated and considered separately from the shear wall in the A-models.

A key feature of the A-model of the shear wall is the use of the subpanels for the sheathing. Verification results for this approach, i.e. Eq. (7), are provided for a  $1.22 \text{ m}$  (4 ft)  $\times$   $2.74 \text{ m}$  (9 ft) shear wall modeled with four subpanels in Fig. 8. A full panel model (using only one pair of interior diagonal truss elements) of the same wall is created for comparison. Shear force in the subpanels are summed for horizontal cuts through the wall in both the lower and upper region and compared with the full panel model in Fig. 8 (b). The subpanel results closely track the full panel model indicating the approach works satisfactorily. In the post-failure regime it is possible that an individual sub-panel will diverge from the single panel solution. In this example, the division of subpanels is arbitrary, but for shear walls in the CFS-NEES building, field studs at their actual locations are modeled as boundary members of subpanels (see Fig. 5(e) or (f) of South elevation as an instance). The above process can be automated to determine the backbone curve of each truss member for every subpanel, but the increased number of nonlinear elements leads to additional modeling effort and computational cost.

In the A-models the framing members are explicitly included. Individual failure modes of all framing members (studs, joists, track, etc.) under each internal force component are incorporated in nonlinear uniaxial materials, as detailed in the modeling of the gravity walls in Section 3.3. Composite action in built-up members, such as shear wall chord studs, is ignored. Also in the A-models, shear anchors (low velocity fasteners (LVFs)) between the bottom track and the foundation are included. The LVFs are assumed to resist base shear with limited pullout capacity and are modeled

as pins between the foundation and the bottom track, mid-distance between studs at  $30.48 \text{ cm}$  (12 in.) spacing. Weak axis bending of the track is very low, thus limiting the pullout stiffness of the LVFs in the model.

Shear wall hold-downs in the A-models are explicitly included using nonlinear axial springs. The backbone response of the Simpson S/HDU6 hold-down, Fig. 9(a), is estimated from industry reported testing [27,32] in tension and assumed to be high in bearing/compression. Highly unsymmetrical nonlinear backbone curves can deteriorate model convergence, to mitigate this the response is modeled with a pair of parallel springs as depicted in Fig. 9(b). Pinching4 and EPP-Gap uniaxial materials model the tension and compression branch respectively. For elastic models (free vibration, linear static and time history) a stiffness of  $2k_{HD}$  (compare with Fig. 9(a)) is employed. The linear stiffness is set to  $2k_{HD}$  so that the pair of elastic hold-downs creates the same amount of induced lateral displacement with the pair of nonlinear hold-downs for small deflection. This treatment assumes the foundation is rigid.

In A-models and 3D P-models of the archetype building, connections are conservatively modeled as fixed for the consideration of simplicity. More importantly, modeling the strap tie between chord studs across floor diaphragm as fixed overestimates the connection stiffness of the tie and it forms a direct load path of gravity load from top floor to the foundation. The error introduced by this modeling idealization may need to be quantified in the future.

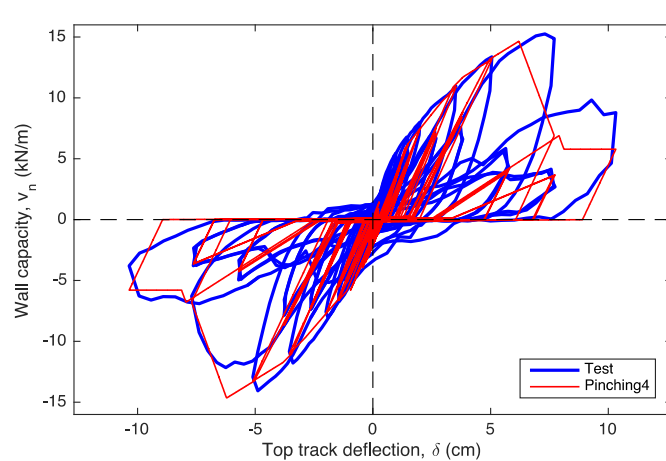
### 3.3. Modeling of gravity walls – CFS framing only

The gravity walls of the CFS-NEES building consists of CFS studs attached to top and bottom track with small bridging channels for weak-axis bracing of the studs. The studs are sized for tributary loads and eccentricity from the ledger-framed floor system is considered. The beneficial influence of sheathing on bracing the studs is ignored in design. The in-plane lateral stiffness of the walls before and after sheathing is ignored in design. P-models ignore the gravity walls, A-models, which aim to realistically simulate the actual building behavior, should include the incidental lateral stiffness that results due to the actual framing members and connections, as well as the additional lateral stiffness and capacity introduced into the system when gravity members are sheathed for the purposes of exterior or interior finish.

Since the gravity system in the A-models can potentially carry lateral loads it is important to include member failure modes in the models for the studs. Ideally, each CFS member could be mod-



(a) Isolated shear wall test



(b) Shear wall response and characterization

Fig. 7. Description of shear wall response characterization.

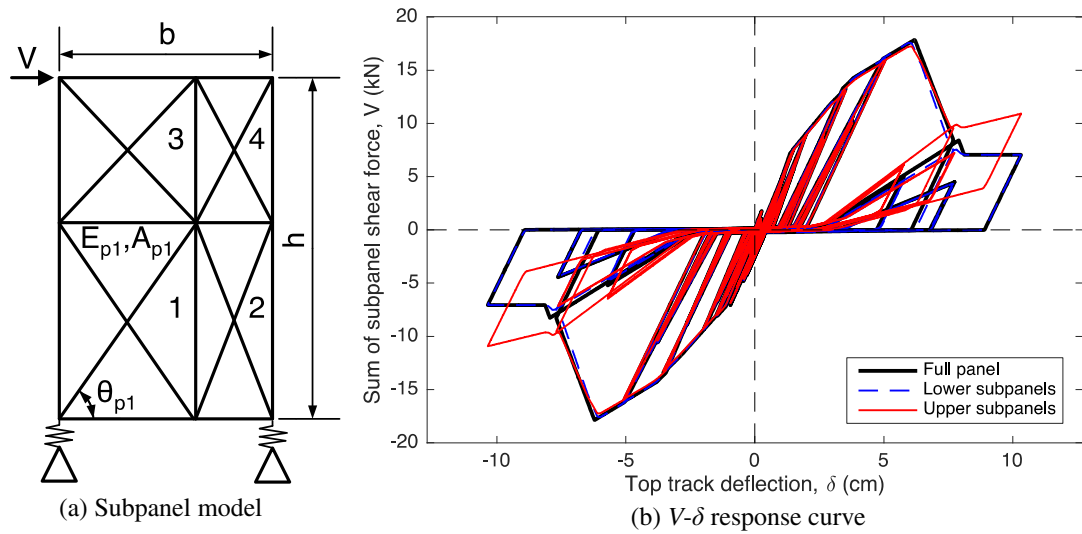


**Fig. 8.** A 1.22 m (4 ft)  $\times$  2.74 m (9 ft) shear wall modeled with subpanels and its  $V - \delta$  response curve.

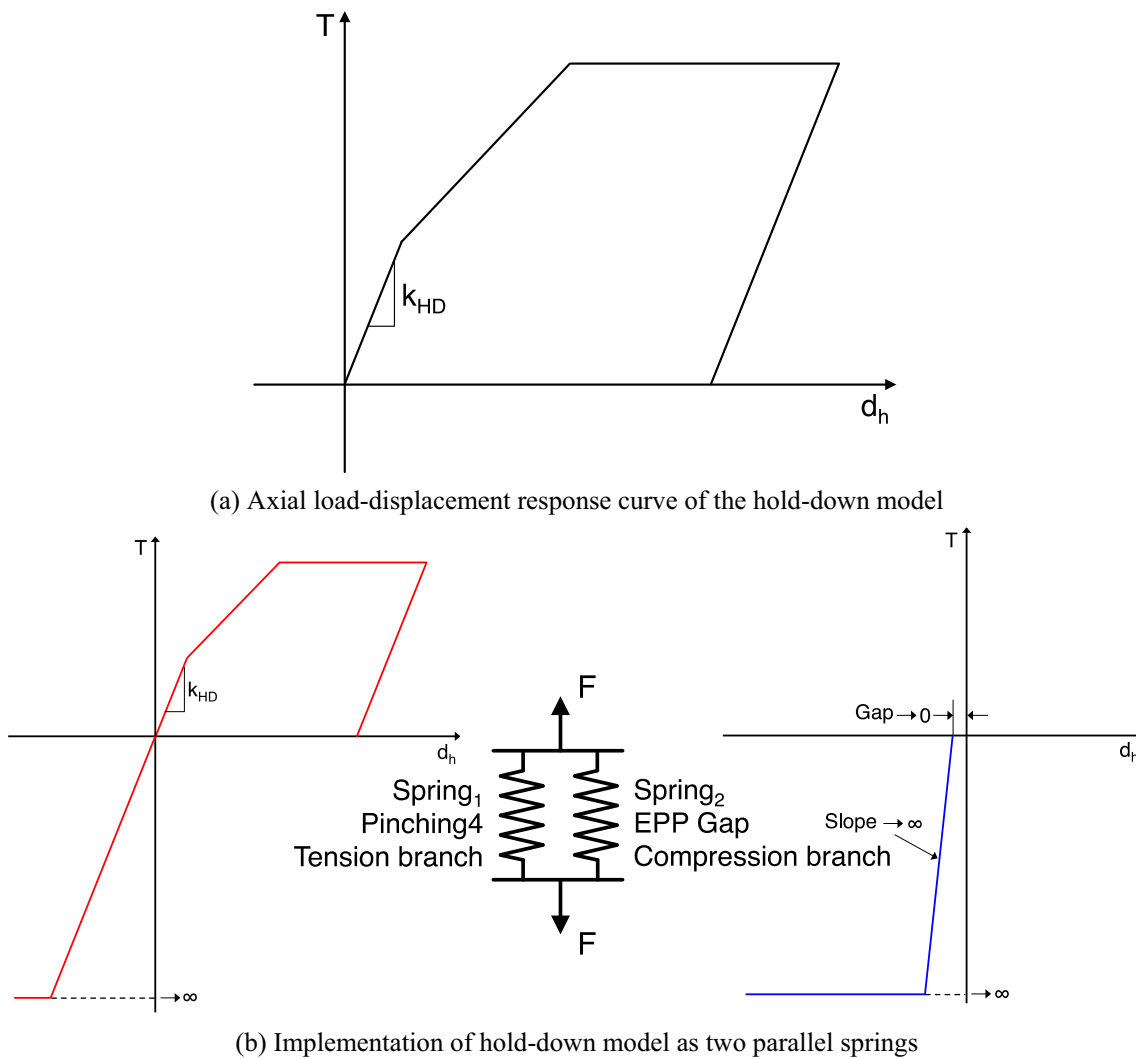


**Fig. 9.** Implementation of Pinching4 material model of the axial response of the hold-down.

**Table 2**

Uniaxial material types and properties in section aggregator of CFS studs.

Load type	Material type	Stiffness	Peak capacity
Axial force, $P$	EPP	$EA$	$T_n (+), P_n (-)$
Strong axis moment, $M_z$	EPP	$El_z$	$M_{nz}$
Weak axis moment, $M_y$	EPP	$El_y$	$M_{nyt} (+), M_{nyc} (-)$
Torque, $T$	Elastic	$GJ$	$\infty$

eled with its complete nonlinear hysteretic response. Recent work on the backbone moment-rotation behavior of cold-formed steel beams [33] and testing on the complete cyclic response of CFS columns and beams [34,35] provides a robust path for the future. However, introduction of these models come at computational cost and their development occurred at the same time as the model employed herein. The approach taken here is to limit the axial, major-axis, and minor-axis bending capacity of the CFS members to their nominal capacity [36] when considered as a fully sheathed member in AISI S100 [3]. This is completed by defining a unique material limit in the fiber element model of each CFS member under each action and using the 'section aggregator' element in OpenSees to combine these uniaxial materials together for a given section, such that the developed members can resist force and moments only up to their code specified nominal capacities.

**Table 2** lists the uniaxial material types and properties used in the section aggregator for CFS studs [27]. Compressive force and bending moment can cause buckling failure, so capacities  $P_n$ ,  $M_{ny}$  and  $M_{nz}$  are computed using the local buckling critical load  $P_{cr}$ ,  $M_{cry}$ ,  $M_{crz}$  available from CFSEI technical note G103-11 [36] and the Direct Strength Method [3] as implemented in AISI S100 [3]. In this manner, local and distortional buckling of any CFS cross-section is captured by uniquely limiting the plastic capacity of the section under each action. For Phase 1 and 2a models of the building since the gravity framing is unsheathed the stud capacities are further reduced to account for distortional buckling [27]. For minor axis bending, the value of  $M_{cry}$  differs when the flange lips are in compression or tension and this is accounted for in the capacities. For tension the yield load  $T_n = F_y A_g$  is employed. The response curve for weak axis bending moment is provided in Fig. 10(a). With this approach we insure that no framing element can develop forces beyond their expected specification nominal strength. The section aggregator in OpenSees works on diagonal terms of element stiffness matrix only and cannot generate any interaction. However, a posteriori design checks on studs of pushover analysis results of 3D A-models show that failures of studs are mostly axial force or single axis bending dominated, see the first authors thesis for further discussion [27]. Again, coupling between lipped channels

in built-up members is ignored for simplicity; they are idealized as multiple individual members at the same location.

Modeling the foundation conditions for the gravity walls is another important consideration in the A-models for accurately predicting the flow of forces in the building. First floor studs are seated in track and bear directly on the foundation; therefore, a stiff bearing load path in compression needs to be considered. The bottom track has low velocity fasteners (LVFs) that connect it to the foundation; the LVFs are essentially mid-distance between studs. Thus, the only load path for uplift of a stud includes minor-axis bending of the track connected to a potentially unreliable (in tension) LVF. The result for the vertical load path of a stud in a gravity wall is a stiff compression load path and a weak tension load path, resulting in an important nonlinearity that must be incorporated into the model. The axial response curve, Fig. 10(b), is realized by an elastic multi-linear uniaxial material attached to spring elements in OpenSees. The material has no energy dissipation under cyclic loading, but it has greatly different stiffness in tension and compression. The LVFs are also modeled as pins, but always located mid-distance between studs. The consequence of these modeling assumptions is that the gravity system can also resist lateral load – a phenomena directly observed in testing, but typically ignored in modeling.

### 3.4. Modeling of gravity walls – CFS-framing with OSB and gypsum sheathing

In Phase 2b the gravity walls are sheathed with exterior OSB, and in Phase 2c interior gypsum board (see Fig. 5(c)–(f)). From the building experiments it is observed that this sheathing significantly increases the building stiffness. To date, little is known about the lateral resistance of sheathed gravity walls in CFS-framed buildings and current design ignores this influence. We estimated the stiffness and backbone curve of sheathed gravity walls using the fastener-based models developed by the CFS-NEES team [20–23] as a surrogate for testing. This surrogate model is driven by nonlinear response recorded from cyclic fastener testing on the same details used in the CFS-NEES building [37]. Fig. 11 depicts the procedure for the  $V - \delta$  response characterization: surrogate models are developed with the correct fastener spacing and framing details for the gravity walls of the CFS-NEES building; monotonic  $V - \delta$  response is obtained from pushover analysis. For this purpose, a 2.44 m (8 ft) by 2.74 m (9 ft) gravity wall with #8 fasteners at 15.24 cm (6 in.) spacing on board edges and 30.48 cm (12 in.) spacing in the field of a board is modeled using this approach and its backbone curve determined as provided in

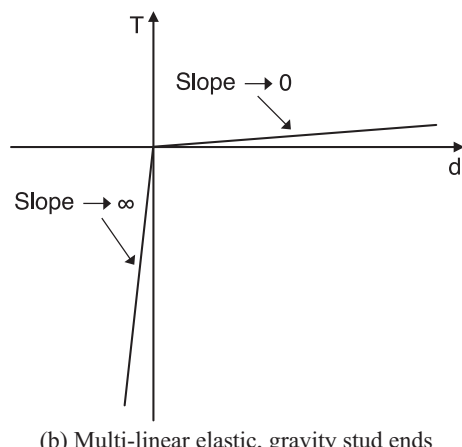
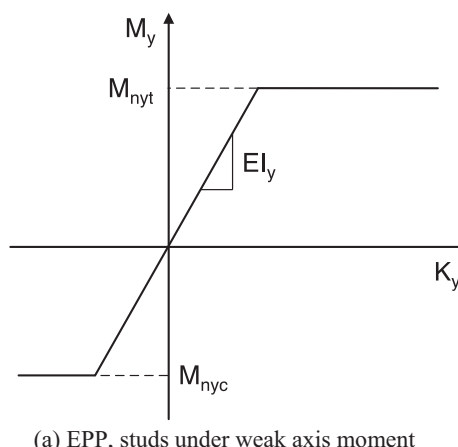
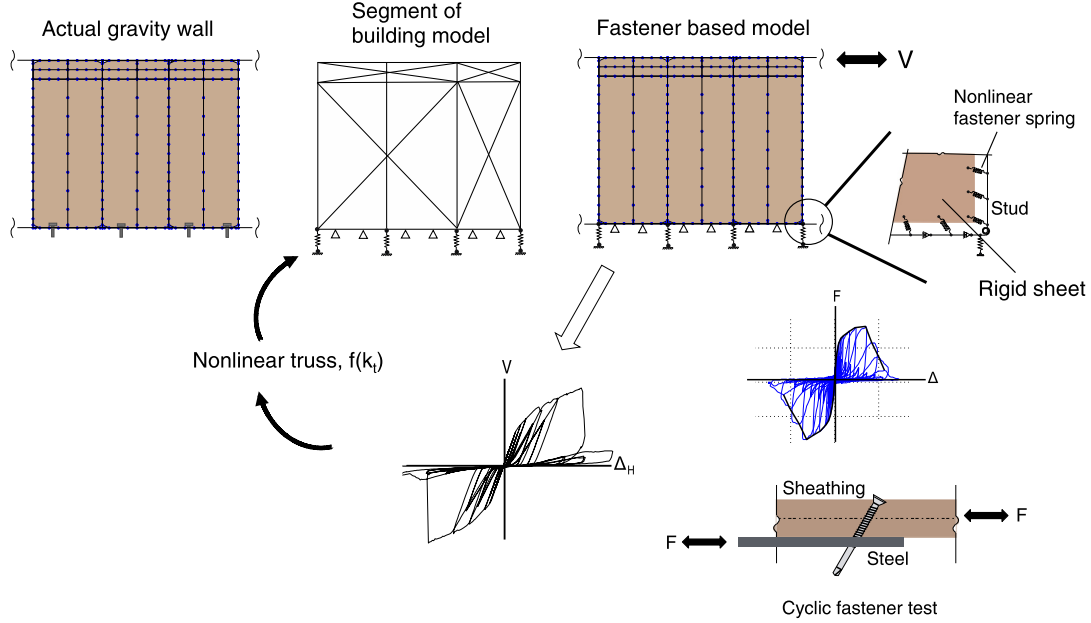
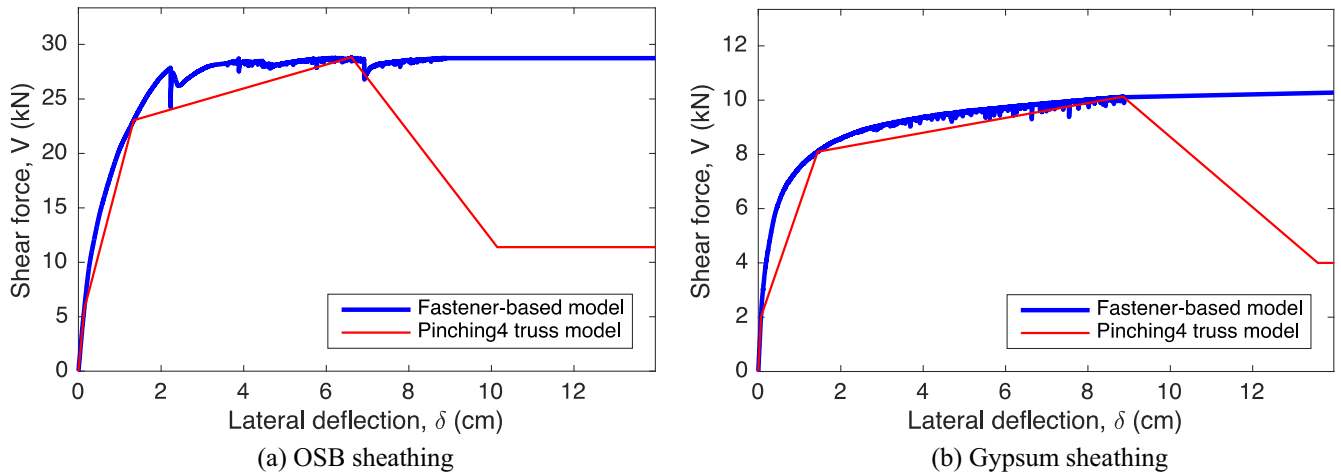


Fig. 10. Typical uniaxial response models in CFS gravity frame modeling.



**Fig. 11.** Development of  $V - \delta$  relationship from surrogate fastener-based models.



**Fig. 12.** Comparison between backbone curves of a sheathed 2.44 m (8 ft)  $\times$  2.74 m (9 ft) gravity wall using fastener-based model and characterized Pinching4 truss model.

**Fig. 12.** The capacities of the OSB and gypsum sheathing are determined as 11.82 kN/m (810 plf) and 4.15 kN/m (285 plf). The backbone curve is then characterized as a Pinching4 material in the same way as the shear walls and discretized into subpanels. Parameters for the pinching effect are kept the same as with the tested shear walls (see the post-peak drop in Fig. 7) due to the shortage of test data; see [27] for all parameters. Interior gypsum sheathing is handled by including a second set of interior truss elements. Note, for gravity walls the connection to foundation remains the same as previously described: significant stiffness exists in compression (bearing), but only very limited resistance exists for tension – therefore, the lateral gravity wall stiffness and strength (which is relatively high) is actually realized in series with these nonlinear foundation conditions and is coupled to the shear walls and other gravity walls based on the actual framing details. This modeling approach for gravity walls is a rational extension of the work on shear walls, and is partially validated by the comparisons made herein; however additional validation and sensitivity studies are appropriate for future efforts adopting this approach as the gravity walls have an important influence on the response.

### 3.5. Modeling of diaphragms

In the 3D models the diaphragm was either considered as rigid or semi-rigid. The semi-rigid diaphragm models for the floor and roof are depicted in Fig. 13(a) and (b). Compared with the 3D explosive drawing of diaphragm framing in Fig. 3 and plan views in Fig. 13(c) and (d), the models correctly capture the out-to-out dimensions of the real diaphragms and include appropriate openings. The diaphragm shear stiffness was included as diagonal truss elements in the plane of the sheathing, framing members including joists and ledger track are positioned 15.24 cm (6 in.) below the diaphragm plane (at their centroid) since the web depth of joists and ledger tracks is 30.48 cm (12 in.) (See cross sections in Fig. 4 for sheathed diaphragms). Strap blocking, as detailed in Fig. 17(e) is extended to allow subdivision of the sheathing panel into subpanels. Nodes that are 15.24 cm (6 in.) apart vertically are connected using two-node link and rigid link elements so they have the same translations but their three rotation DOFs are weakly coupled to approximate the connection stiffness between very deep

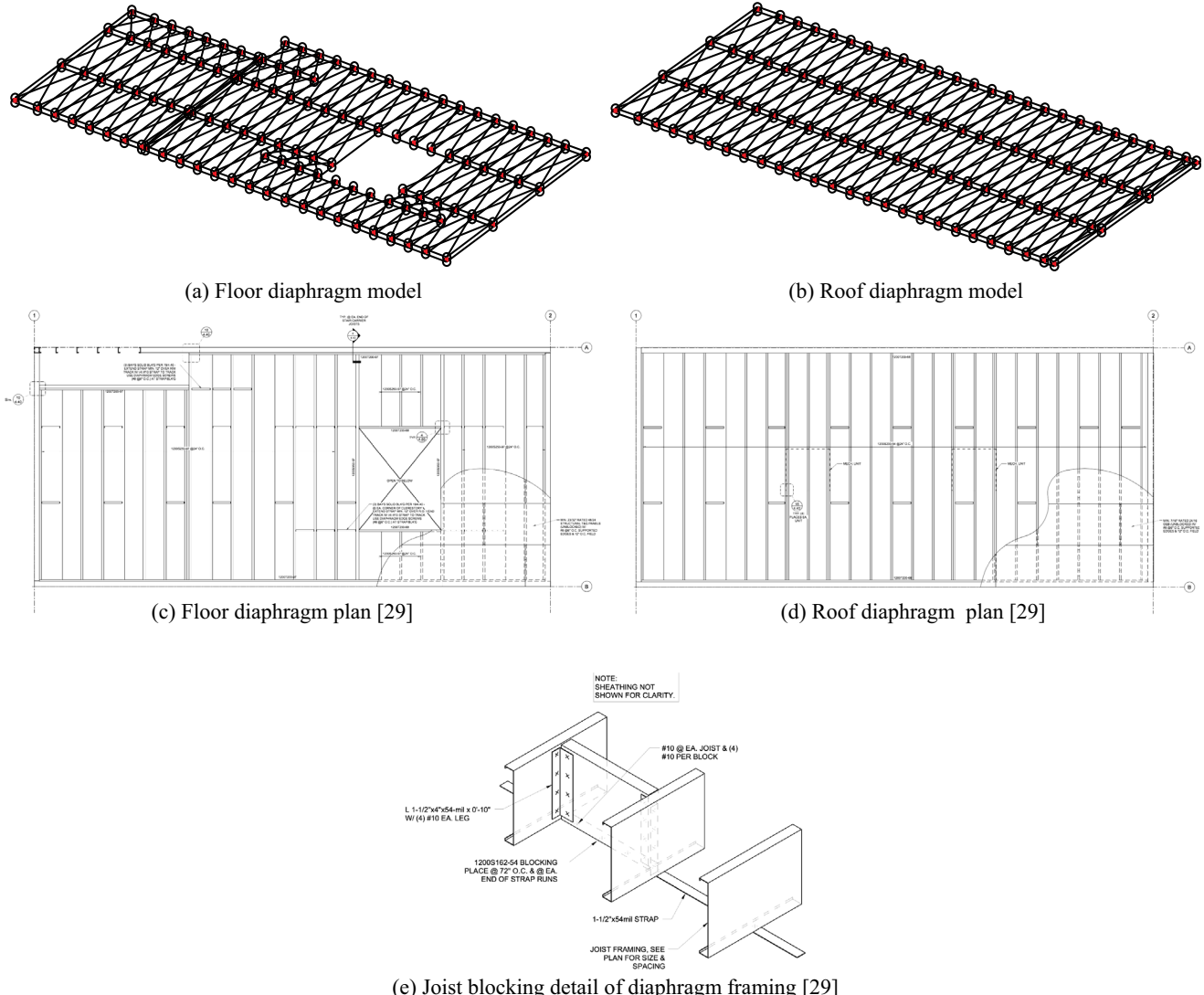


Fig. 13. Semi-rigid diaphragm OpenSees FE models and design drawings.

CFS joists and ledger tracks and sheathing panels fastened to them from above.

No test data exists for the shear-deformation response of the diaphragm so the shear wall Pinching4 hysteretic model was adjusted using engineering judgment to develop the diaphragm semi-rigid shear response. The sheathing employed in the floors is thicker than in the walls: 1.83 cm (23/32 in.) vs. 1.11 cm (7/16 in.). The APA panel design specification [38] reports that the thicker sheathing has a shear stiffness 1.53 times greater than the thinner, and this value was used to increase the tangent stiffness in the model. All other strength and pinching parameters utilized the values derived for shear walls (with hold-down deformations removed). As provided in Table 3, we compared the response of our semi-rigid diaphragm model to Eqn. D2.1-1 in AISI S213 [6] for unblocked diaphragms at a force level based on the design diaphragm shear. The heuristic approximation of the semi-rigid diaphragm behavior is reasonably aligned with the approximate expression in AISI S213: the numbers are of the same order, and the maximum discrepancy is about 60%. The semi-rigid diaphragm model is integrated in the high fidelity A-models through Phase 1 to Phase 2c. For Phase 2d, due to the fact that the locations of interior partition walls do not always align with

**Table 3**

Comparison of peak lateral displacement between diaphragm models and design equation.

Level	Direction of load	$\Delta$ of FE model (cm)	$\Delta$ of Eqn. D2.1-1 [6] (cm)
Floor	Short	0.279	0.452
Floor	Long	0.079	0.084
Roof	Short	0.191	0.488
Roof	Long	0.061	0.094

steel members of the subpanel diaphragm, only the rigid diaphragm model was employed.

### 3.6. Modeling of interior walls

For the Phase 2d model of the CFS-NEES building the interior partition walls are considered. The resulting model of the isolated interior walls is illustrated in Fig. 14. Each wall is modeled as two nonlinear diagonals. For interior walls on the floor level, the stud end bearing boundary condition is included. No lateral constraints to the foundation are applied, thus the interior walls cannot resist base shear, but they can support overturning of exterior walls wherever they meet (see Fig. 1(b)) and thereby contributes to the

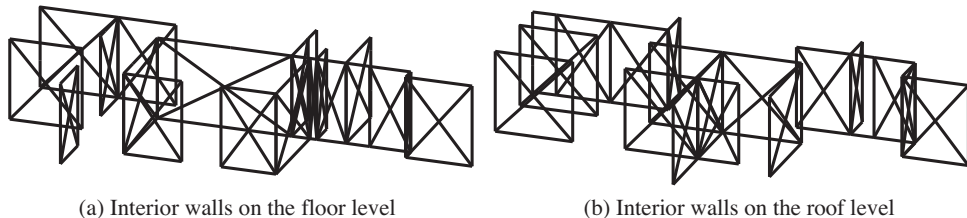


**Fig. 14.** Interior wall FE models in OpenSees.

lateral resistance. In the CFS-NEES building, interior walls are framed with nonstructural CFS studs and sheathed with gypsum boards. The gravity wall surrogate model with gypsum sheathing, as described in Section 3.4, was utilized to approximate the nonlinear response and implemented as Pinching4 material parameters in the diagonals framing the partition walls.

### 3.7. Distribution of seismic mass and gravity load

The 35,100 kg (77,500 lbs) seismic mass is constant through all phases of modeling. For the state-of-the-practice (P)-models, as shown in Fig. 5(a), the mass is equally distributed to four corner nodes on the rigid diaphragm at floor and roof level. For the state-of-the-art (A)-models, as shown in Fig. 5(b)–(f), the supplemental mass in the test specimen is distributed to nodes on the track where the diaphragm plane meets the wall line (consistent with the end of joist locations). Gravity load of the building is applied separately and is proportional to seismic nodal mass by the acceleration of gravity,  $g$ .

## 4. Validation of models and comparison with full-scale shake table test results

### 4.1. Brief overview of full-scale shake table test results and terminology in model validation

Full-scale testing of the CFS-NEES archetype building was conducted in the summer of 2013 on the shake tables of the University at Buffalo [8–10]. The testing was conducted in two primary phases: Phase 1 and 2. The Phase 1 building, with structural components only (Fig. 4(a)), was tested through the three-axis Canoga Park record (16%, 44% and 100% levels) from the 1994 Northridge earthquake. At 100% scale the ground motion is essentially equal to the Design Basis Earthquake (DBE) per U.S. standards [5,29] for this building. The new Phase 2 building was constructed after the deconstruction of Phase 1 and was tested nondestructively at intermediate phases. The complete Phase 2e building (Fig. 4(f)) was subjected to the 100% Canoga Park record, and then to the three-axis near-field Rinaldi record at 100%, also from the 1994 Northridge earthquake. The 100% Rinaldi record is equivalent to the Maximum Considered Earthquake (MCE) per U.S. standards [5,39] for this building. System identification tests using 0.1 g white-noise signals were performed at each phase to determine the building's natural periods and damping before and after the scaled ground motion tests.

Response of the building was recorded by an extensive sensor array [8]. Key recorded outputs from the tests include story/building drifts, load cell axial forces in the shear wall hold-downs (Fig. 2 (b)), and acceleration amplification factors [8]. A major observation from the tests is that the stiffness, damping, and response of the building are significantly altered by systems not typically assumed to contribute to lateral response. The first mode period in the long direction of the building decreases from 0.32 s in Phase 1 to 0.15 s in Phase 2e. Measured damping prior to large excitation testing

increases from 3.75% in Phase 1 to 8.00% in Phase 2e. Under seismic testing both the Phase 1 and Phase 2e buildings experienced minimal drift and returned to straight after excitation. For the Phase 2e building, the story drift under 100% Rinaldi was less than 1% and damage only occurred in the interior non-structural walls [2]. These imply that the building is stiffer and stronger than engineering designs suggest and the building benefits greatly from components not typically assumed to contribute to the response.

The developed high-fidelity P- and A- models are subjected to free vibration analysis and time history analysis to assess their validity (see Table 1 and Fig. 5(b)–(d)). All time history analyses are second-order inelastic (i.e. material and geometric nonlinear), with Rayleigh damping ratio set to 5%. The chosen damping is close to pre-test damping of the structure, but kept uniform across phases to isolate this influence as well as to match specifications and the design spectrum. The excitations in the time history analysis are not the original ground motion records (as plotted in [10]) but rather the recorded accelerations experienced by the CFS-NEES building during testing at the same scale level as the tested phase. The experienced acceleration is different from the targeted acceleration 'loaded' into the shake table to excite the structure due to the tuning of the shake table. The difference in experienced vs. intended peak ground acceleration (PGA) can be larger than 50% in the worst cases, as depicted in [8]. The nomenclature for the excitations is the abbreviation for the ground record: CNP for Canoga Park, or RRS for Rinaldi, followed by the scale level (in%). Natural periods are directly available from free vibration analysis, and story drifts, nodal acceleration and hold-down axial forces are determined from outputs of the conducted time history analyses.

### 4.2. Comparison of natural periods

Table 4 and Fig. 15 summarize the first natural period ( $T_1$ ) in the long and short direction obtained from system identification tests and as predicted by the models for each construction phase. Note the measured decrease in  $T_1$  from the structural only Phase 1 building to the complete Phase 2d/2e building. Given fixed mass this period decrease implies a  $4.5\times$  increase in long direction building lateral stiffness and  $1.9\times$  increase in the short direction. These increases occur, even though none of the additional phases 2b–2e are specifically intended to increase stiffness. In addition, it is important to note that even the unsheathed gravity wall system has a pronounced impact on the predicted period (stiffness): compare the P-model (Phase 0 in Fig. 15) to the Phase 1/2a A-model. The predicted first mode period from the models indicates these large increases in the building stiffness are largely captured in the A-models. The match is best in the long direction, where the difference in natural period is typically less than 3%, while error in the short direction is 5–10%, and modestly, but consistently over-predicts the short direction stiffness. Major sources of error include the conservative estimation of connection stiffness as fixed, the accuracy of stiffness estimate of gravity and interior wall sheathing and semi-rigid diaphragms as subpanels and the

**Table 4**

First natural periods in long and direction from system identification test and model prediction.

Phase	Model	Long		Short		
		T <sub>1</sub> (s), Test	T <sub>1</sub> (s), Model	T <sub>1</sub> (s), Test	T <sub>1</sub> (s), Model	
0	P	P-3D-RD-b	0.32	0.50	0.36	0.66
1/2a	A	A1-3D-SD-a	0.32	0.30	0.36	0.32
2b	A	A2b-3D-SD-a	0.20	0.22	0.30	0.28
2c	A	A2c-3D-SD-a	0.17	0.18	0.27	0.23
2d	A	A2d-3D-RD-a	0.16	0.17	0.25	0.22
2e	A	A2d-3D-RD-a	0.15	0.17	0.26	0.22

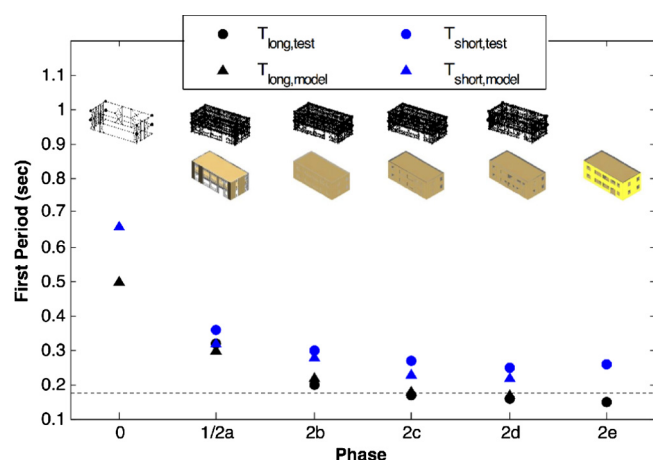


Fig. 15. Comparison of the first mode period between buildings and state-of-the-art models.

approximation of built-up members as isolated ones, etc. However, subsystem level test needs to be performed before we can quantify these errors.

#### 4.3. Comparison of story drifts

Peak story drift in the long ( $u$ ) and short ( $v$ ) directions for the first (subscript  $1$ ) and second (subscript  $2$ ) stories, normalized by story height,  $h$ , is summarized for the testing and the P- and A-series models in Table 5. Excitation and response is three-dimensional so the average of displacement values in the corners of the building are employed to measure the drift of the story, in the same manner as the data was experimentally processed (see [27] and [37]). The state-of-the-practice (P)-model, which fully considers the nonlinear shear wall response, but only the shear wall response, fails to provide a reasonable prediction of the building drift. The magnitude of predicted peak story drift from the A-models matches adequately with the tests; the greatest error is experienced for the DBE-level (100% CNP) excitation of the Phase 1 (structural only) building, where the model predicts a peak story drift 0.5% greater than experienced in the test.

Time history of the story drift response for the large excitation records are provided in Fig. 16 for the A-series models and the corresponding tests. For example, the A-model for the Phase 1 (structural only) building with a DBE-level (100% CNP) excitation had the largest error and this can be observed in Fig. 16(a). The time history data indicates that the absolute error in the first story ( $u_1$ ) is not as important as the systematic error in the second story ( $u_2$ )

**Table 5**

Comparison of maximum percent story drift across phases and ground motions.

Phase	Ground Motion	Long direction					
		Δu <sub>1</sub> /h (%)			Δu <sub>2</sub> /h (%)		
		Test	P-Model <sup>a</sup>	A-Model <sup>b</sup>	Test	P-Model <sup>a</sup>	A-Model <sup>b</sup>
1	44% CNP	0.56	1.00	0.47	0.38	-0.64	0.13
2b	44% CNP	0.19	"	0.19	0.12	"	-0.08
2c	44% CNP	0.14	"	0.17	0.11	"	0.08
2d	44% CNP	0.13	"	0.10	0.08	"	0.05
2e	44% CNP	0.10	"	-0.09	0.06	"	0.04
1	100% CNP	1.18	5.09	1.66	0.81	-0.78	-0.55
2e	100% CNP	0.27	"	0.42	0.16	"	0.14
2e	16% RRS	0.11	0.61	0.06	0.07	0.35	0.03
2e	100% RRS	0.69	12.14	0.84	0.43	9.14	-0.34
Short direction							
		Δv <sub>1</sub> /h (%)			Δv <sub>2</sub> /h (%)		
		Test	P-Model <sup>a</sup>	A-Model <sup>b</sup>	Test	P-Model <sup>a</sup>	A-Model <sup>b</sup>
		-0.36	-0.32	0.27	0.29	-0.30	-0.11
1	44% CNP	-0.29	"	0.28	0.20	"	0.11
2b	44% CNP	0.22	"	0.21	0.17	"	-0.09
2c	44% CNP	0.19	"	0.23	0.15	"	0.10
2e	44% CNP	0.19	"	-0.16	0.14	"	0.08
1	100% CNP	-0.85	-3.57	0.88	-0.57	1.45	0.34
2e	100% CNP	0.47	"	0.37	0.32	"	0.19
2e	16% RRS	0.16	-0.50	-0.09	-0.11	-0.39	0.04
2e	100% RRS	0.73	-10.73	0.99	-0.50	-3.96	0.52

<sup>a</sup> State-of-the-practice P-3D-RD-b model.

<sup>b</sup> State-of-the-art A1-3D-SD-a, A2b-3D-SD-a, A2c-3D-SD-a, A2d-3D-RD-a models.

prediction. In fact, second story drift predictions are consistently lower across the models. All models employ an idealized connection across the floor, ignoring the flexibility introduced by the CFS strap that ties the shear wall chord studs across the two stories (see Fig. 2(d)). This additional flexibility impacts the predicted drifts in the second story; however this impact decreases in later construction phases [27]. In addition, the 100% CNP test experienced damage in a second story chord stud due to a construction error where a built-up stud was replaced by a single stud [8] and this condition

was not re-created in the model. Comparison for the Phase 2d/2e A-model is favorable, as provided in Fig. 16(b) and (c).

#### 4.4. Comparison of load cell (hold-down) force and the distribution

In the shake table testing load cells were placed on the anchor rod of the shear wall hold-downs as indicated in Fig. 2(c) and detailed in [8]. The load cells can indicate the extent of tension in the anchor rods, and indicate the presence of compression at

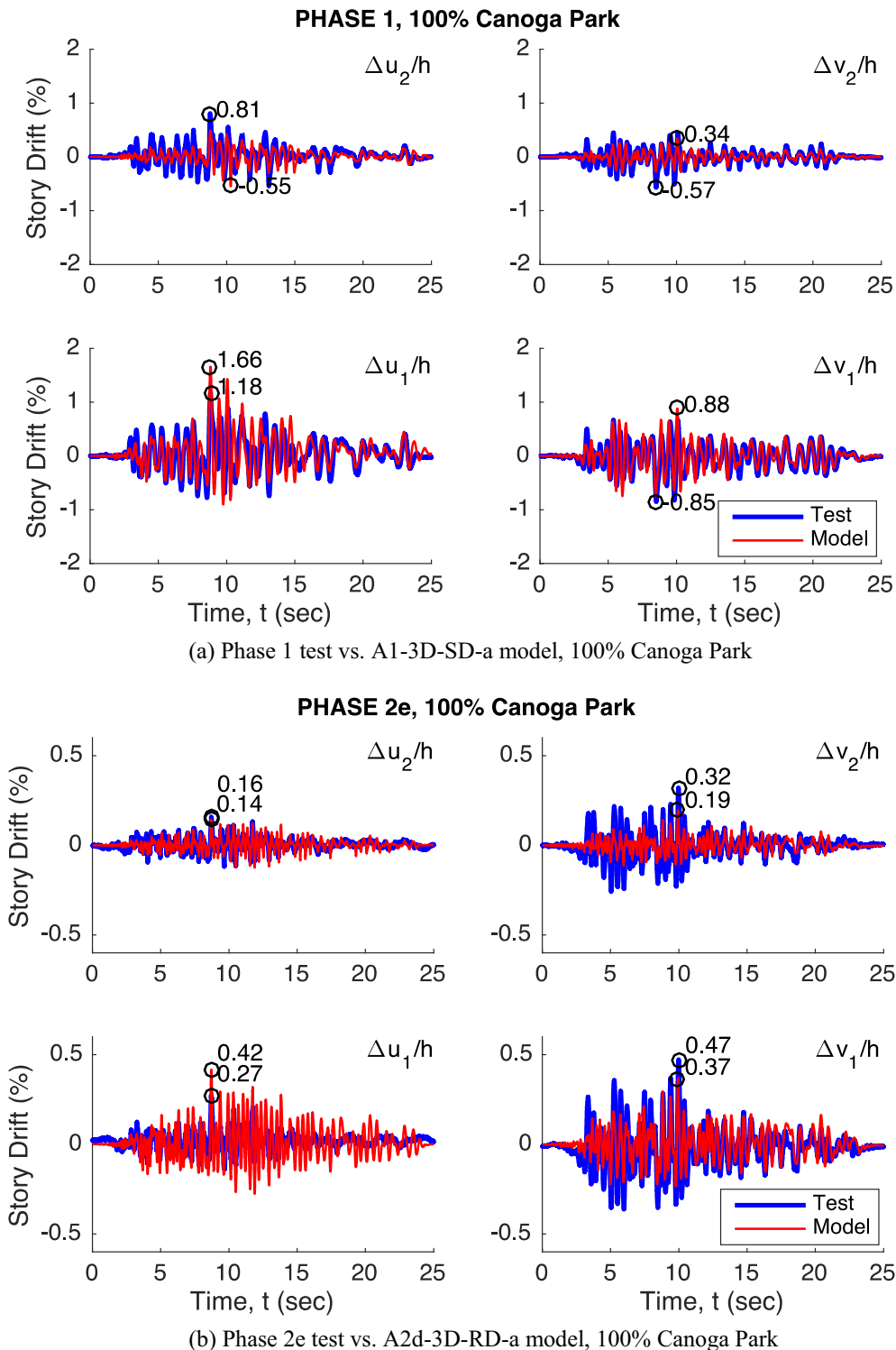


**Fig. 16.** Comparison of time history plots of story drift.

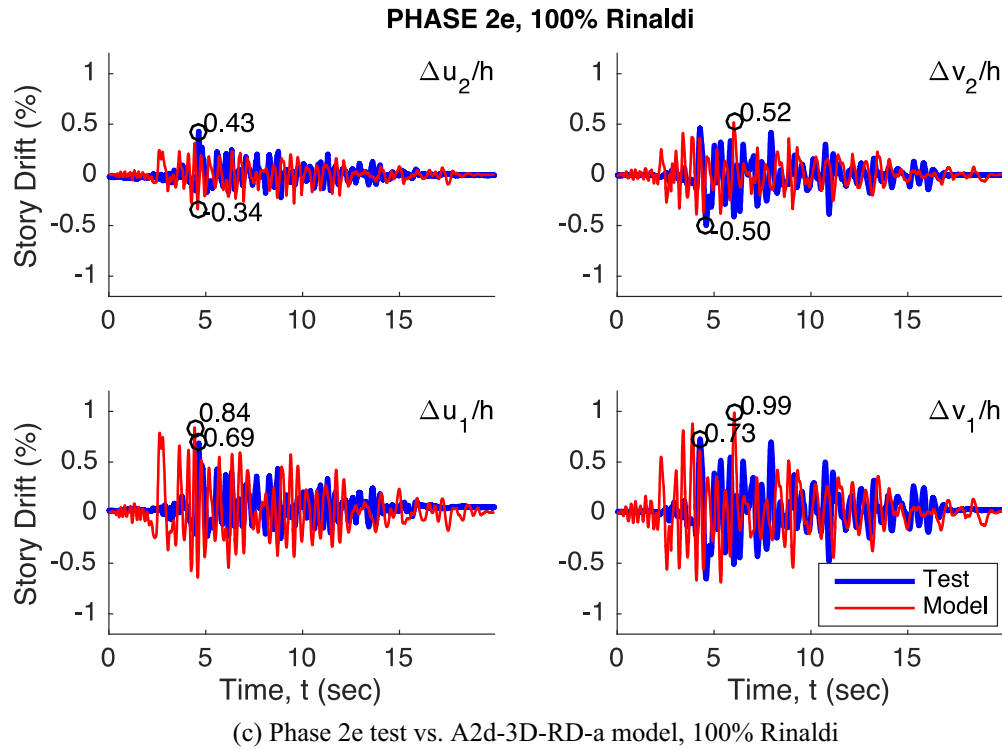


Fig. 16 (continued)

**Table 6**

Comparison of peak hold-down tensile force across phases and ground motions.

Phase	Motion	Wall L1S1 at Load Cell (LC) 5			Wall L1W1 at Load Cell (LC) 8		
		Peak hold-down tensile force (kN)			Peak hold-down tensile force (kN)		
		Test	P-model <sup>a</sup>	A-Model <sup>b</sup>	Test	P-model <sup>a</sup>	A-Model <sup>b</sup>
1	44% CNP	4.50	32.34	9.45	7.10	25.58	3.74
2b	44% CNP	3.19	"	5.90	2.42	"	2.54
2c	44% CNP	2.42	"	6.07	2.13	"	3.00
2d	44% CNP	1.65	"	4.49	1.87	"	3.92
2e	44% CNP	1.71	"	4.78	1.63	"	3.84
1	100% CNP	14.59	41.59	14.53	13.85	52.76	7.77
2e	100% CNP	3.93	"	8.64	4.09	"	4.08
2e	16% RRS	1.70	25.76	2.79	2.01	33.90	2.94
2e	100% RRS	7.73	45.95	12.42	9.12	42.61	9.98

<sup>a</sup> State-of-the-practice P-3D-RD-b model.<sup>b</sup> State-of-the-art A1-3D-SD-a, A2b-3D-SD-a, A2c-3D-SD-a, A2d-3D-RD-a models.

least up to the pre-tension force applied at installation. The distribution of the measured hold-down forces during earthquake excitations is detailed in [8–10] and comparison of the model predictions across all load cells are provided in [27]. Here two shear wall hold-down load cells (LCs) in the southwest corner of the building (LC5 and LC8 as indicated in Fig. 3) are selected for detailed comparison between the models and testing, peak forces are provided in Table 6 and selected time histories in Fig. 17.

The P-models, which allow only the shear walls to carry lateral load, drastically over-predict the shear wall hold-down forces across all earthquakes and construction phases. For example, in the long direction under DBE-level (100% CNP) testing on the structural-only (Phase 1/2a) building the hold-down forces are over-predicted by 3×, this increases to 10× for the completed (Phase 2e) building, and remains as high as 6× even for the MCE-level (100% RRS) excitation. The A-models are far better than the P-models; but agreement, particularly with the peak forces, is

not perfect. As Table 6 shows, the A-models typically over-predict the hold-down force, but not near as drastically as the P-model. The sensitivity of the peak hold-down force to the construction phase is greater in reality than in the A-model predictions; particularly in the short-direction of the building. Hold-down predictions for the strong motion excitations (100% CNP, 100% RRS) are more accurate than forces at lower excitations and generally align with measured response, but still with considerable error. Comparison of the time series of the hold-down forces, Fig. 17, provides additional insights: the A-models include more high frequency content than the test results (i.e., more rapid fluctuation of the predicted axial force in Fig. 17(b) and (c)), comparing only peak forces is a limited metric for building response, and the A-model predicts modest residual force (permanent drift) in the hold-downs for Phase 2e that is not observed in the testing. Detailed comparison of load cell axial force at other/lower excitation levels is available in [27]. For smaller excitations, the accuracy in the A-models' axial

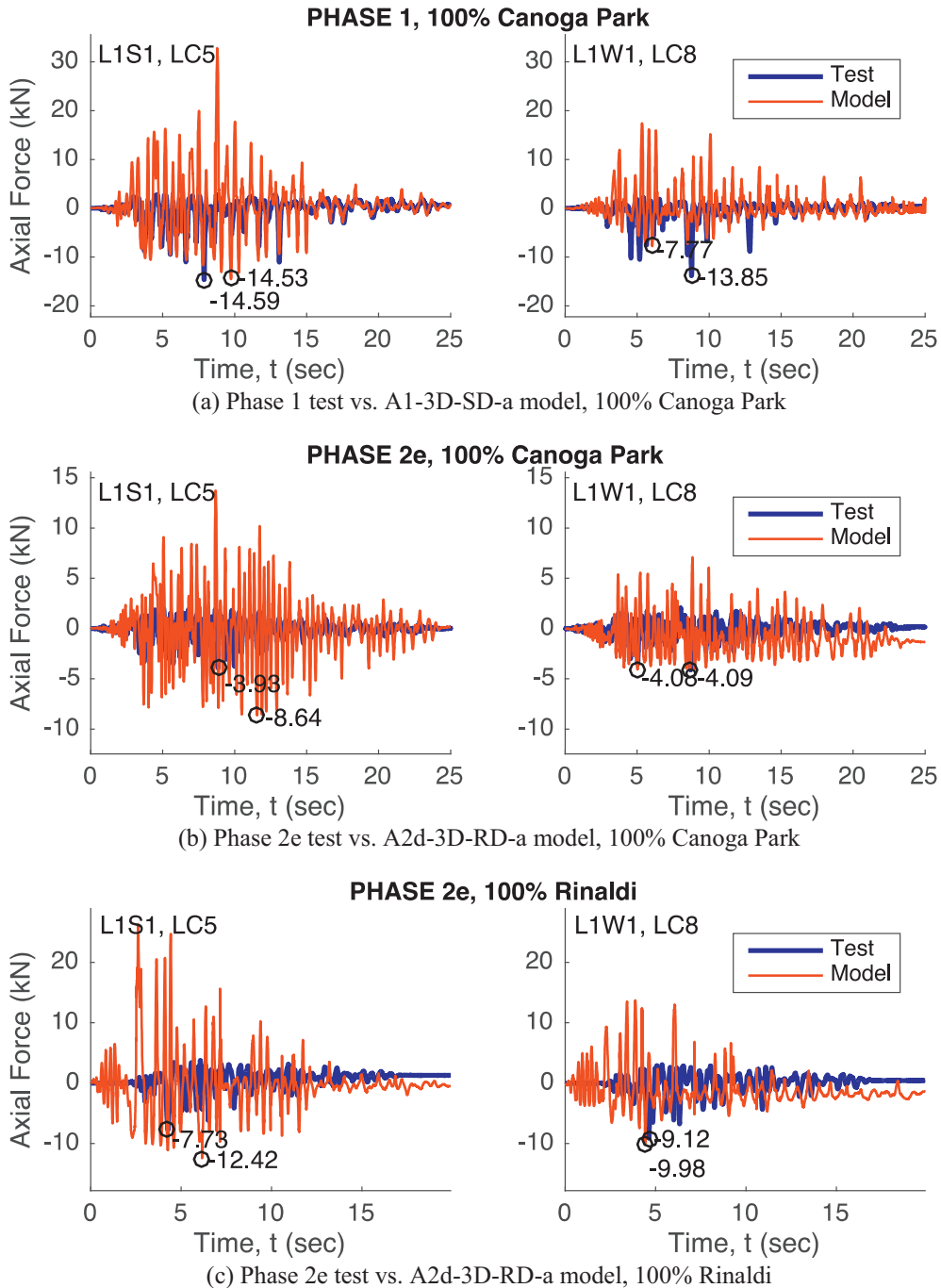


**Fig. 17.** Comparison of time history plots of selected load cells.

force prediction is better and coincidence of the peak value with the experimental curve is improved since the nonlinear effect in the response curve (bearing vs. tension) at the hold-down is less significant. In total, it is clear that the A-models provide improved prediction of hold-down forces over conventional models and predictions, but the accuracy further indicates that improvement in modeling, particularly of vertical load paths that lead to these hold-down forces would be beneficial in the long term.

#### 4.5. Comparison of peak story acceleration

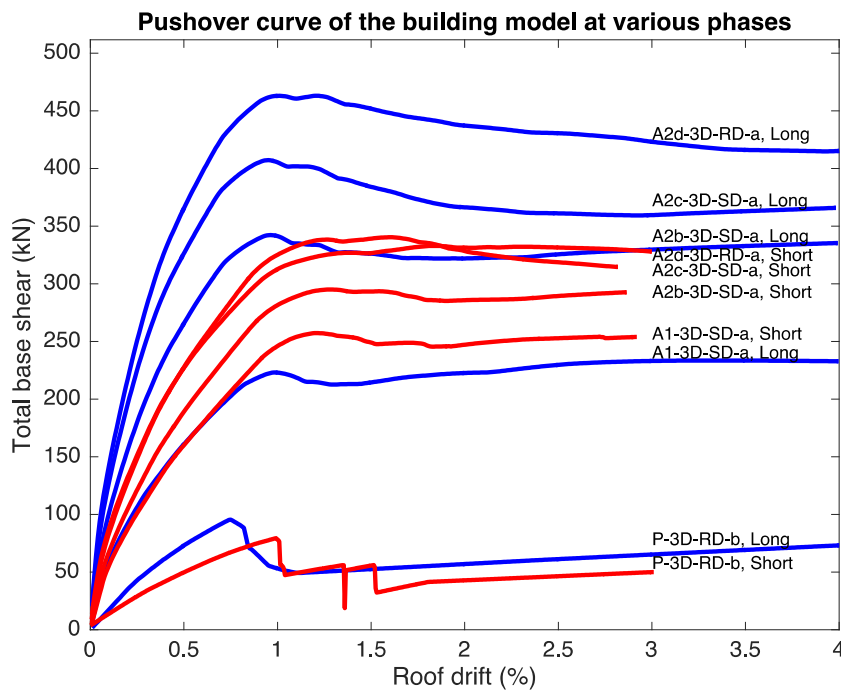
In the shake table testing accelerometers were placed throughout the building as detailed in the sensor plan [8]. Comparisons of the measured peak story accelerations in the long and short

building directions with the model predictions are provided in Table 7. The P-models under-predict the accelerations during strong motion excitations (100% CNP, 100% RRS). The A-models typically over-predict the peak accelerations during strong motion excitations, and have particular error in the MCE-level (100% RRS) excitation. The trend of the peak acceleration across the construction phases (as the building is completed) is generally down in the experiments (compare Phase 1 to 2e for 44% CNP), while the A-model predicts increased accelerations across the same phases. In the experiments the damping increased with construction phase, but in the models the damping is held constant at 5%, this is one possible source for this discrepancy. Examination of the time history of the A-model for 100% RRS excitation indicates the large acceleration errors are associated with convergence problems in

**Table 7**

Comparison of peak story acceleration in g across phases and ground motions.

Phase	Ground Motion	Long direction							
		Base a (g)			Floor a (g)			Roof a (g)	
		Test	P-Model <sup>a</sup>	A-Model <sup>b</sup>	Test	P-Model <sup>a</sup>	A-Model <sup>b</sup>	Test	P-Model <sup>a</sup>
1	44% CNP	0.185	0.368	0.407	0.422	0.631	0.422	0.506	
2b	44% CNP	"	0.325	"	0.501	0.385	"	0.588	
2c	44% CNP	"	0.329	"	0.628	0.392	"	0.703	
2d	44% CNP	"	0.314	"	0.416	0.392	"	0.491	
2e	44% CNP	"	0.294	"	0.428	0.373	"	0.477	
1	100% CNP	0.420	1.280	0.382	0.787	1.834	0.371	1.116	
2e	100% CNP	"	0.816	"	0.984	0.965	"	0.988	
2e	16% RRS	0.132	0.252	0.256	0.302	0.325	0.252	0.363	
2e	100% RRS	0.825	1.646	0.656	3.590	1.923	0.659	5.196	
Short direction									
Phase	Ground Motion	Base a (g)			Floor a (g)			Roof a (g)	
		Test	P-Model <sup>a</sup>	A-Model <sup>b</sup>	Test	P-Model <sup>a</sup>	A-Model <sup>b</sup>	Test	P-Model <sup>a</sup>
		0.157	0.274	0.328	0.487	0.399	0.323	0.683	
1	44% CNP	"	0.231	"	0.603	0.344	"	0.659	
2b	44% CNP	"	0.227	"	0.654	0.339	"	0.638	
2c	44% CNP	"	0.202	"	0.443	0.350	"	0.486	
2d	44% CNP	"	0.211	"	0.361	0.361	"	0.467	
2e	44% CNP	"	0.592	0.424	0.763	0.995	0.533	0.910	
1	100% CNP	"	0.503	"	0.462	0.863	"	0.717	
2e	16% RRS	0.078	0.133	0.154	0.227	0.178	0.162	0.263	
2e	100% RRS	0.487	0.734	0.614	7.080	1.063	0.524	13.156	

<sup>a</sup> State-of-the-practice P-3D-RD-b model.<sup>b</sup> State-of-the-art A1-3D-SD-a, A2b-3D-SD-a, A2c-3D-SD-a, A2d-3D-RD-a models.**Fig. 18.** Comparison of pushover curves of selected models.

the vertical load elements: bearing at the stud ends and at the hold-down locations. In addition the vertical load path at the floors is simpler in the models than in the actual construction. The drastic change in tension/compression stiffness in these elements coupled with large vertical excitations in the excitation record lead to errors in acceleration predictions; however, building drift approximations are still adequate. More robust means for modeling such large stiffness changes are desirable.

## 5. Application and discussion

The primary application of the state-of-the-art “A”-models is the development and validation of seismic response modification coefficients, via the FEMA P695 [40] procedure, for use in Equivalent Lateral Force design. Although that larger effort is part of a separate study, some modest application of the developed models in this direction is provided here. The overstrength of a system can

**Table 8**

Comparison of peak building base shear across phases and ground motions.

Phase	Motion	Peak building base shear $V_b$ (kN)										
		Long direction				Short direction						
		P-model <sup>a</sup>	A-Model <sup>b</sup>	P-model <sup>a</sup>	A-Model <sup>b</sup>	SW <sup>c</sup> only	SW <sup>c</sup>	Other	Total	SW <sup>c</sup> only	SW <sup>c</sup>	Other
1	Pushover	95.5	183.7	49.8	233.5	79.3	206.1	51.2	257.2	206.1	51.2	257.2
2b	"	"	179.9	162.3	342.3	"	220.1	74.9	295.0	220.1	74.9	295.0
2c	"	"	211.4	195.9	407.3	"	250.6	89.8	340.3	250.6	89.8	340.3
2d/e	"	"	259.0	204.1	463.1	"	258.3	74.6	332.9	258.3	74.6	332.9
1	100% CNP	93.4	191.5	37.8	229.3	73.8	160.3	24.1	184.5	160.3	24.1	184.5
2b	"	"	119.8	117.7	237.5	"	134.9	45.1	180.0	134.9	45.1	180.0
2c	"	"	121.0	119.4	240.4	"	143.5	49.4	192.9	143.5	49.4	192.9
2d/e	"	"	136.2	108.6	244.8	"	149.6	42.7	192.4	149.6	42.7	192.4
1	100% RRS	97.4	199.9	34.2	234.1	82.7	184.6	30.8	215.4	184.6	30.8	215.4
2b	"	"	181.6	161.3	342.9	"	181.2	56.9	238.2	181.2	56.9	238.2
2c	"	"	191.7	186.8	378.5	"	215.9	69.0	284.8	215.9	69.0	284.8
2d/e	"	"	213.5	172.7	386.2	"	219.0	56.2	275.3	219.0	56.2	275.3

<sup>a</sup> State-of-the-practice P-3D-RD-b model.<sup>b</sup> State-of-the-art A1-3D-SD-a, A2b-3D-SD-a, A2c-3D-SD-a, A2d-3D-RD-a models.<sup>c</sup> SW = Shear wall.

be approximated through a pushover analysis. Provided in Fig. 18 is the pushover analysis results for the P- and A-models across construction phases. Recall the design base shear is 49 kN. The models illustrate how stiffness and strength increases during construction and the wide gap between the best approximation of nonlinear response in the P-model and the best prediction of the actual response in the A-models. As discussed further in [10] the P-models are useful for design idealization purposes today and when coupled with existing design procedures ([3], [5]–[7]) ultimately result in a building with good performance, but they are not aligned with observed performance. Table 8 provides the peak base shear associated with these pushover results along with the peak base shears recorded in the strong motion simulations. Additional break down and discussion of the base shear results are provided in [27]. Note, in the testing no direct prediction of the peak base shear is possible. An estimation of base shear from shaking table test is determined from the inertial force of a 2-DOF system without damping in Tables 3–7 of [8]. It estimates the base shear of Phase 1 building under 100% CNP is 317.0 kN in long direction and 176.6 kN in short direction. For Phase 2e building under 100% CNP, the estimates are 455.5 kN and 204.4 kN. For Phase 2e building under 100% RRS, the estimates are 814.0 kN and 306.7 kN. The experimental estimates of base shear are larger than simulation results in Table 8 due to the absence of damping but show the consistent trend of significant increase from Phase 1 to Phase 2e. The predicted overstrength in the complete system is considerable, and as high as 7 in the short direction and 9 in the long direction.

Overall, CFS-NEES testing indicated that the seismic response of CFS-framed buildings is significantly influenced by the behavior of the complete building system. The modeling detailed herein provides a means to include the key elements of this complete system response in a realistic building-scale model. Further comparison of models at more fidelity levels and analysis results under load cases not tested are covered in [27] and modeling preference is summarized. In order to more accurately capture the stiffness and capacity of the lateral system, shear walls and gravity walls should be modeled with high fidelity; characterized backbone response curves from test results should be applied wherever possible; pinching effect should be included for better modeling of the system's energy dissipation; three dimensional coupling should be present, but rigid diaphragm model can be adopted for simplicity. Comparison between the developed models and the testing demonstrates

that overall the developed models capture the key behavior and changes in response, but even with the relatively high level of model complexity improvements are possible. In particular, the vertical load path could be refined to better reflect the flexibility of the shear wall chord stud floor-to-floor tie. Use of higher damping values may also be appropriate; however, as discussed in FEMA P-750 [41], this may require additional justification.

## 6. Conclusions

This paper provides explanation and validation for state-of-the-art modeling of the seismic response of cold-formed steel (CFS) repetitively-framed buildings with oriented strand board (OSB)-sheathed shear walls and floors. The developed models are aligned with shake table tests that indicate significant contributions in lateral stiffness, strength, and damping from the CFS-framed gravity system, as well as non-structural finishes and systems. The paper also explicitly demonstrates that even the best state-of-the-practice models: ones that employ nonlinear time history analysis with nonlinear hysteretic models of the CFS-framed shear walls, are still poor predictors of actual building performance and therefore a poor choice for developing seismic response modification coefficients for use in design. The developed state-of-the-art building model includes a number of key features. All CFS members are explicitly modeled with capacity appropriate for local or distortional buckling limit states as dictated by sheathing conditions. The impact of sheathing on lateral stiffness is included through nonlinear diagonal truss elements within the CFS framing. The nonlinear hysteretic response of the diagonal truss elements is determined by testing (e.g. direct shear wall tests), or by surrogate modeling based on the tested nonlinear cyclic response of steel-fastener-sheathing connector tests. Foundation conditions reflect actual response with stiff bearing load paths at the end of studs (i.e. all studs, not just shear wall chord studs) and tension load paths with experimentally determined stiffness at hold-down locations. The models are three-dimensional and include a semi-rigid diaphragm consisting of CFS joists and nonlinear diagonal truss elements approximating the OSB-sheathed floor system. CFS ledger members, which are an important part of the floor gravity system and diaphragm system, are explicitly modeled. The end result of the state-of-the-art approach is a model that adequately predicts the stiffness, strength, and local response when compared with

testing. Given that the complete building response is as much as 16 times stiffer and 9 times stronger than response based on isolated shear walls, these modeling details are necessary and important. Areas for improvement in the model are identified, particularly with respect to the vertical load path across the floor. The developed model provides an approach for modeling CFS-framed buildings that is consistent with seismic performance-based design evaluations. In addition, the developed model provides a means to more fully explore the response of CFS-framed buildings and quantify the contribution of non-traditional lateral systems in this framing typology. Finally, the developed modeling protocol provides a means to assess and develop seismic response modification coefficients for CFS repetitively-framed buildings using the P695 procedure, a key objective for future work.

## Acknowledgements

The authors would like to thank the National Science Foundation [NSF-CMMI #1041578], American Iron and Steel Institute (AISI), ClarkDietrich, Steel Stud Manufacturers Association, Steel Framing Industry Association, Devco Engineering (notably Rob Madsen and Phil Clark), Mader Construction, DSi Engineering, Simpson Strong-Tie and the members of the Industrial Advisory Board: Renato Camporese, Thomas A. Castle, Kelly Cobeen, L. Randy Daudet, Richard B. Haws, Jay Parr, and Steven B Tipping, and additional Industry Liaisons: George Frater, Don Allen, Tom Lawson, and Fernando Sessma. The views expressed in this work are those of the authors and not NSF, AISI, or any of the participating companies or advisors.

## Appendix A. Supplementary materials

Supplementary data associated with this article can be found, in the online version, at <https://doi.org/10.1016/j.engstruct.2017.10.008>.

## References

- [1] Hancock G. Cold-formed steel structures: research review 2013–2014. *Adv Struct Eng* 2016;19(3):393–408.
- [2] Schafer BW, Ayhan D, Leng J, Liu P, Padilla-Llano DA, Peterman KD, et al. Seismic response and engineering of cold-formed steel framed buildings. *Structures* 2016.
- [3] American Iron and Steel Institute. North American specification for the design of cold-formed steel structural members, 2012 edition. AISI S100-12 ed. Washington, DC: American Iron and Steel Institute; 2012.
- [4] European Convention for Constructional Steelwork. Eurocode 3: Design of steel structures, Part 1-3: General rules – Supplementary rules for cold-formed members and sheeting. Brussels, Belgium: European Convention for Constructional Steelwork; 2007.
- [5] American Society of Civil Engineers. Minimum design loads for buildings and other structures. ASCE/SEI 7-05 ed. Reston, VA: American Society of Civil Engineers; 2005.
- [6] American Iron and Steel Institute. North American standard for cold-formed steel framing - lateral design 2007 edition with supplement no. 1 and commentary. AISI S213-07-SI-09 ed. Washington, DC: American Iron and Steel Institute; 2009.
- [7] American Iron and Steel Institute. North American Standard for Seismic Design of Cold-Formed Steel Structural Systems. AISI S400-15 ed. Washington, DC: American Iron and Steel Institute; 2016.
- [8] Peterman KD. Behavior of full-scale cold-formed steel buildings under seismic excitations. Baltimore, MD: Johns Hopkins University; 2014.
- [9] Peterman KD, Stehman MJ, Madsen RL, Buonopane SG, Nakata N, Schafer BW. Experimental seismic response of a full-scale cold-formed steel framed building: sub-system level response. *J Struct Eng* 2016.
- [10] Peterman KD, Stehman MJ, Madsen RL, Buonopane SG, Nakata N, Schafer BW. Experimental seismic response of a full-scale cold-formed steel framed building: system-level response. *J Struct Eng* 2016.
- [11] Leng J, Schafer BW, Buonopane SG. Seismic computational analysis of CFS-NEES building. In: Proc. 21st international specialty conference on cold-formed steel structures; 2012.
- [12] Leng J, Schafer BW, Buonopane SG. Modeling the seismic response of cold-formed steel framed buildings: model development for the CFS-NEES building. In: Proc. annual stability conference-structural stability research council; 2013.
- [13] McKenna F. Open system for earthquake engineering simulation (OpenSees). Berkeley, CA: Pacific Earthquake Engineering Research Center; 2011.
- [14] Shamim I, Rogers CA. Numerical modeling and calibration of CFS framed shear walls under dynamic loading. In: Proc. 21st international specialty conference on cold-formed steel structures; 2012.
- [15] Yu C, Yu G, Wang J. Innovative cold-formed steel framed shear wall sheathed with corrugated steel sheets: experiments and dynamic analysis. In: Proc. 22nd international specialty conference on cold-formed steel structures; 2014.
- [16] Fiorino L, Iuorio O, Landolfo R. Seismic analysis of sheathing-braced cold-formed steel structures. *Eng Struct* 2012;34:538–47.
- [17] Fülop LA, Dubina D. Performance of wall-stud cold-formed shear panels under monotonic and cyclic loading: Part II: Numerical modelling and performance analysis. *Thin Wall Struct* 2004;42(2):339–49.
- [18] Dubina D. Behavior and performance of cold-formed steel-framed houses under seismic action. *J Constr Steel Res* 2008;64(7):896–913.
- [19] Li Y, Ma R, Shen Z. Numerical simulation on dynamic behavior of a cold-formed steel framing building test model. In: Proc. 22nd international specialty conference on cold-formed steel structures; 2014.
- [20] Buonopane SG, Bian G, Tun TH, Schafer BW. Computationally efficient fastener-based models of cold-formed steel shear walls with wood sheathing. *J Constr Steel Res* 2015;110:137–48.
- [21] Bian G, Buonopane SG, Ngo H, Schafer BW. Fastener-based computational models with application to cold-formed steel shear walls. In: Proc. 22nd international specialty conference on cold-formed steel structures; 2014.
- [22] Bian G, Padilla-Llano DA, Leng J, Buonopane SG, Moen CD, Schafer BW. OpenSees modeling of cold-formed steel framed wall system. In: Proc. 8th international conference on behavior of steel structures in seismic areas; 2015.
- [23] Bian G, Padilla-Llano DA, Buonopane SG, Moen CD, Schafer BW. OpenSees modeling of wood sheathed cold-formed steel framed shear walls. In: Proc. annual stability conference-structural stability research council; 2015.
- [24] van de Lindt JW. Evolution of wood shear wall testing, modeling, and reliability analysis: bibliography. *Pract Period Struct Des Construct* 2004;9(1):44–53.
- [25] van de Lindt JW, Pei S, Liu H, Filiault A. Three-dimensional seismic response of a full-scale light-frame wood building: numerical study. *J Struct Eng* 2010;136(1):56–65.
- [26] Christovasilis IP, Cimellaro GP, Barani S, Foti S. On the selection and scaling of ground motions for fragility analysis of structures. In: Proc. 2nd European conference on earthquake engineering and seismology; 2014.
- [27] Leng J. Simulation of cold-formed steel structures. Baltimore, MD: Johns Hopkins University; 2015.
- [28] International Code Council. International Building Code. 2009th ed. Washington, DC: International Code Council; 2009.
- [29] Madsen RL, Nakata N, Schafer BW. CFS-NEES building structural design narrative. 2011;CFS-NEES-RR01.
- [30] Lowes LN, Altontash A. Modeling reinforced-concrete beam-column joints subjected to cyclic loading. *J Struct Eng* 2003;129(12):1686–97.
- [31] Liu P, Peterman KD, Schafer BW. Impact of construction details on OSB-sheathed cold-formed steel framed shear walls. *J Constr Steel Res* 2014;101:114–23.
- [32] Simpson Strong-Tie Company Inc., Load table of S/H/DU Holdowns; 2013.
- [33] Ayhan D, Schafer BW. Moment-rotation characterization of cold-formed steel beams. 2012;CFS-NEES-RR02.
- [34] Padilla-Llano DA, Moen CD, Eatherton MR. Cyclic flexural hysteretic models for cold-formed steel seismic simulation. In: Proc. European conference on steel and composite structures; 2014.
- [35] Padilla-Llano DA. A framework for cyclic simulation of thin-walled cold-formed steel members in structural systems. Blacksburg, VA: Virginia Polytechnic Institute and State University; 2015.
- [36] Li Z, Schafer BW. Tabulated local and distortional elastic buckling solutions for standard shapes; 2011;TN-G103-11.
- [37] Peterman K, Nakata N, Schafer B. Hysteretic characterization of cold-formed steel stud-to-sheathing connections. *J Constr Steel Res* 2014;101:254–64.
- [38] APA—The Engineered Wood Association. Panel design specification. Tacoma, WA: APA—The Engineered Wood Association; 2012.
- [39] American Society of Civil Engineers. Minimum design loads for buildings and other structures. ASCE/SEI 7-10 ed. Reston, VA: American Society of Civil Engineers; 2010.
- [40] Applied Technology Council. Quantification of building seismic performance factors. 2009;FEMA P695.
- [41] Building Seismic Safety Council. NEHRP recommended seismic provisions for new buildings and other structures. 2009;FEMA P750.